Available online at www.sciencedirect.com
ScienceDirect
International Journal of Heat and Fluid Flow 28 (2007) 1227–1243
International Journal of HEAT AND FLUID FLOW
www.elsevier.com/locate/ijhff

A complete and irreducible dynamic SGS heat-flux modelling based on the strain rate tensor for large-eddy simulation of thermal convection

Bing-Chen Wang [a,*], Jing Yin [b], Eugene Yee [a], Donald J. Bergstrom [b]

[a] Defence Research and Development Canada – Suffield, P.O. Box 4000, STN Main, Medicine Hat, AB, Canada T1A 8K6
[b] Department of Mechanical Engineering, University of Saskatchewan, Saskatoon, SK, Canada S7N 5A9

Received 8 November 2006; received in revised form 31 May 2007; accepted 1 June 2007
Available online 20 July 2007

Abstract

In this paper, a general family of explicit algebraic tensor diffusivity functions based on the resolved temperature gradient vector and strain rate tensor is studied and applied to the construction of new constitutive relations for modelling the subgrid-scale (SGS) heat flux (HF). Based on Noll's formulation, dynamic linear and nonlinear tensor diffusivity models are proposed for large-eddy simulation of thermal convection. The constitutive relations for these two proposed models are complete and irreducible. These two new models include several existing dynamic SGS HF models as special cases. It is shown that in contrast to the conventional modelling approach, the proposed models embody more degrees of freedom, permit non-alignment between the SGS HF and resolved temperature gradient vectors, reflect near-wall flow physics at the subgrid scale, and therefore, allow for a more realistic geometrical representation of the SGS heat flux for large-eddy simulation of thermal convection. Numerical simulations have been performed using a benchmark test case of a combined forced and natural convective flow in a vertical channel with a Reynolds number of $Re_\tau^a = 150$ and a Grashof number of $Gr = 9.6 \times 10^5$. The results obtained using the two proposed SGS HF models are compared with reported direct numerical simulation (DNS) data as well as predictions obtained using several conventional dynamic SGS HF models.

Keywords: Turbulence; Heat transfer; Convection; Large-eddy simulation; Subgrid-scale model

1. Introduction

With recent advances in computational technology and the introduction of dynamic SGS modelling for closure of the filtered momentum equation by Germano et al. (1991) and Lilly (1992), large eddy simulation (LES) has become a promising tool for investigating turbulent heat and fluid flows. The application of LES to turbulent scalar transport processes requires modelling of the SGS scalar flux vector for closure of a filtered scalar transport equation. LES of thermal convection using the dynamic modelling approach began with the works of Moin et al. (1991), Cabot (1992), Sullivan and Moeng (1992), and Wong and Lilly (1994) in the early 1990s. The dynamic SGS HF model proposed in these seminal works is based on the concept of a SGS eddy thermal diffusivity, and will be referred to as the *dynamic eddy diffusivity model for representing the SGS heat flux* (DEDM-HF). The DEDM-HF is based on a linear constitutive relation, analogous to Fourier's law for describing molecular heat conduction, and assumes that the SGS HF vector (i.e., h_j) is instantaneously proportional to and aligned with the negative resolved temperature gradient, viz. $h_j \propto -\partial\bar{\theta}/\partial x_j$. Obviously, this simplified linear constitutive relation is inconsistent with the physics of turbulent convection, and cannot correctly reflect the geometrical properties of the SGS HF vector. In spite of these deficiencies, the DEDM-HF is the most popular dynamic SGS HF model in use and has been successfully applied

* Corresponding author. Tel.: +1 403 544 4791; fax: +1 403 544 3388.
E-mail addresses: bingchen.wang@drdc-rddc.gc.ca (B.-C. Wang), jiy080@mail.usask.ca (J. Yin), eugene.yee@drdc-rddc.gc.ca (E. Yee), don.bergstrom@usask.ca (D.J. Bergstrom).

0142-727X/$ - see front matter © 2007 Elsevier Inc. All rights reserved.
doi:10.1016/j.ijheatfluidflow.2007.06.001

Nomenclature

a_j, b_j	base vectors
$\overline{A}_{ij}$	resolved velocity gradient tensor
$\lvert\overline{A}\rvert$	norm of $\overline{A}_{ij}$: $(2\overline{A}_{ij}\overline{A}_{ij})^{1/2}$
$\mathbf{c}$	SGS HF model coefficient vector: $[C_{\theta E}, C_{\theta S}, C_{\theta N}]^{\mathrm{T}}$
C, C_1, C_2	coefficients
c_{P}	specific heat at constant pressure
C_S, C_W, C_N	SGS stress model coefficients
$C_{\theta E}, C_{\theta S}, C_{\theta N}$	SGS heat flux model coefficients
D_{ij}	tensor diffusivity
$\mathscr{E}$	magnitude of the residual vector: $\mathscr{E}_j\mathscr{E}_j$
$\mathscr{E}_j$	residual vector
g_i	gravitational acceleration vector: $[-g,0,0]^{\mathrm{T}}$
Gr	Grashof number: $g\beta\Delta\theta(2\delta)^3/\nu^2$
h_j	grid-level SGS heat flux vector: $\mathbf{h} = [h_j]$
H_j	test-grid-level SGS heat flux vector
$\mathbf{K}$	matrix
L_j	length of the physical domain in the jth direction
$\mathscr{L}_j$	vector
$\mathbf{l}$	vector: $\mathbf{l} = [\mathscr{L}_j]$
$\mathscr{L}_{ij}$	Leonard type stress tensor
M_{ij}, W_{ij}, N_{ij}	differential tensors
P_j, Q_j, R_j	differential vector
p	pressure
q_{w}	wall heat flux
Re_τ	Reynolds number based on friction velocity: $u_\tau\delta/\nu$
$\overline{S}_{ij}$	resolved strain rate tensor: $(\partial\bar{u}_i/\partial x_j + \partial\bar{u}_j/\partial x_i)/2$
$\lvert\overline{S}\rvert$	norm of $\overline{S}_{ij}$: $(2\overline{S}_{ij}\overline{S}_{ij})^{1/2}$
T_τ	friction temperature: $q_{\mathrm{w}}/(\rho c_{\mathrm{P}} u_\tau)$
T_{ij}	test-grid-level SGS stress tensor
u_i	velocity components: $i = 1,2,3$
u_τ	wall friction velocity: $\sqrt{\tau_{\mathrm{w}}/\rho}$
α	molecular thermal diffusivity: $\lambda/(\rho c_{\mathrm{P}})$
$\alpha_{ij}, \lambda_{ij}, \zeta_{ij}$	test-grid-level tensors
α_{sgs}	SGS eddy thermal diffusivity
$\alpha^{\mathrm{e}}_{\mathrm{sgs}}$	effective SGS eddy thermal diffusivity
β	thermal expansion coefficient
$\beta_{ij}, \gamma_{ij}, \eta_{ij}$	grid-level tensors
δ	half channel width
δ_{ij}	Kronecker delta
Δ	mesh or filter size
λ	thermal conductivity
ν	kinematic viscosity
ν_{sgs}	SGS eddy viscosity
$\overline{\Omega}_{ij}$	resolved rotation rate tensor: $(\partial\bar{u}_i/\partial x_j - \partial\bar{u}_j/\partial x_i)/2$
ϕ	a scalar variable
Φ	random alignment angle between h_j and $\partial\bar{\theta}/\partial x_j$
φ	coefficients of a tensor polynomial
ρ	density
θ	temperature
θ_{B}	bulk temperature
Θ_{r}	reference temperature
τ_{w}	wall shear stress
τ_{ij}	grid-level SGS stress tensor

Subscripts and superscripts

$(\cdot)_1$, $(\cdot)_2$, $(\cdot)_3$	streamwise, wall-normal, and spanwise components, respectively
$(\cdot)^{\mathrm{a}}$	quantity averaged over two walls
$(\cdot)_{\mathrm{c}}$	cold wall region
$(\cdot)_{\mathrm{h}}$	hot wall region
$(\cdot)_i$, $(\cdot)_j$, $(\cdot)_{ij}$	vectors or second order tensors: $i, j = 1,2,3$
$(\cdot)^*_{ij}$	a trace-free tensor: $(\cdot)^*_{ij} = (\cdot)_{ij} - (\cdot)_{kk}\delta_{ij}/3$
$(\cdot)_{\mathrm{rms}}$	root-mean-square
$(\cdot)_{\mathrm{sgs}}$	subgrid-scale component
$(\cdot)_{\mathrm{w}}$	value at the wall
$\overline{(\cdot)}$	grid-level filter
$\widetilde{(\cdot)}$	test-grid-level filter
$(\cdot)^+$	wall coordinates
$(\cdot)''$	residual component relative to a time- and plane-averaged quantity
$\langle\cdot\rangle$	time- and plane-averaged quantity

to the prediction of thermal convective flows (Lee et al., 2004; Pallares and Davidson, 2002; Avancha and Pletcher, 2002; Dailey et al., 2003; Keating et al., 2004; Wang and Lu, 2004; Tyagi and Acharya, 2005).

Since the introduction of the DEDM-HF in the early 1990s, a great deal of effort has been made to improve the SGS HF modelling for numerical investigation of theoretical and engineering flows (Kobayashi, 2006). Recently, dynamic SGS HF models have advanced from models of the eddy diffusivity type to those based on a tensor diffusivity in order to improve the physical and geometrical representation of the SGS HF vector. Salvetti and Banerjee (1995) introduced a *two-parameter mixed model for representing the SGS heat flux* (DTPMM-HF), which dynamically combines the linear eddy diffusivity SGS HF model with a scale-similarity SGS HF model. The proposed DTPMM-HF was an extension of the work of Zang et al. (1993) on the dynamic mixed SGS stress model, and has been recently applied by Tyagi and Acharya (2005) for studying heat transfer of rotating rib roughened square duct flow, and by Jaberi and Colucci (2003) for studying reacting and non-reacting turbulent flows using both the *a priori* and *a posteriori* LES methods. By using truncated Taylor series expansions for analysis of filtered flow variables, Porté-Agel et al. (2001a,b) and Kang and Meneveau (2002) introduced a simplified DTPMM-HF, which dynamically combines the linear eddy diffusivity SGS HF model with a gradient SGS HF model. This simplified DTPMM-HF has been applied

to investigation of heat fluxes and dissipation in an atmospheric boundary layer and a heated wind tunnel wake flow using the *a priori* LES approach. Different from the approach of dynamic mixed models, Peng and Davidson (2002) proposed a *dynamic homogeneous linear tensor diffusivity model for representing the SGS heat flux* (DHLTDM-HF) in their study of a buoyancy driven turbulent flow. The DHLTDM-HF replaces the scalar eddy diffusivity of the DEDM-HF with a homogeneous linear tensor diffusivity based on the resolved strain rate tensor, i.e., $h_j \propto -\overline{S}_{jk}(\partial\bar{\theta}/\partial x_k)$. Using the theory of tensor functions, Wang et al. (2007) recently proposed a dynamic inhomogeneous linear tensor diffusivity model (DILTDM-HF) for studying a mixed convective channel flow. The tensor diffusivity for the DILTDM-HF is constructed as an inhomogeneous linear function of the resolved strain rate and rotation rate tensors. Since the unphysical assumption of the parallel alignment between h_j and $-\partial\bar{\theta}/\partial x_j$ as imposed by the DEDM-HF is relaxed, the DTPMM-HF, DHLTDM-HF and DILTDM-HF are expected to provide a more realistic geometrical representation of h_j allowing for non-alignment between the SGS heat flux vector and the resolved temperature gradient, hence improving the physical representation of the SGS scalar transport processes.

In continuum physics, the theory of tensor invariants and functions is essential for modelling the nonlinear constitutive relations required for describing crystal classes, viscoelastic phenomenon and non-Newtonian fluids. The modern development of a rigorous formulation of nonlinear constitutive laws using tensor functions derives largely from the pioneering works of Reiner (1945) and Rivlin (1948) in the late 1940s. Since these seminal works, the mathematical theory of tensor invariants and functions and its application to the formulation of nonlinear constitutive relations have been extensively developed (Spencer, 1971; Zheng, 1994).

The objective of this research is to apply the theory of tensor functions to formulate a new complete and irreducible dynamic nonlinear tensor diffusivity model and also a new general dynamic inhomogeneous linear tensor diffusivity model based on the resolved strain rate tensor and temperature gradient vector for representation of the SGS heat flux. This paper is organized as follows: in Section 2, formulations for two existing and two new dynamic SGS HF models are introduced; in Section 3, the test case and numerical algorithm are described; in Section 4, the results of LES for combined forced and natural convection are analyzed; and finally in Section 5, the major conclusions of this research are summarized.

2. SGS stress and heat flux models

In LES, the filtered continuity, momentum and scalar transport equations take the following form for an incompressible flow:

$$\frac{\partial \bar{u}_i}{\partial x_i} = 0, \tag{1}$$

$$\frac{\partial \bar{u}_i}{\partial t} + \frac{\partial}{\partial x_j}(\bar{u}_i\bar{u}_j) = -\frac{1}{\rho}\frac{\partial \bar{p}}{\partial x_i} + \nu\frac{\partial^2 \bar{u}_i}{\partial x_j \partial x_j} - \frac{\partial \tau_{ij}}{\partial x_j} - \beta g_i(\bar{\theta} - \Theta_r), \tag{2}$$

$$\frac{\partial \bar{\theta}}{\partial t} + \frac{\partial}{\partial x_j}(\bar{u}_j\bar{\theta}) = \alpha\frac{\partial^2 \bar{\theta}}{\partial x_j \partial x_j} - \frac{\partial h_j}{\partial x_j}, \tag{3}$$

where $\bar{\theta}$ represents the filtered scalar (temperature), $[g_j] = [-g,0,0]^T$ is the gravitational acceleration vector, β is the thermal expansion coefficient, α is the molecular thermal diffusivity, Θ_r is the reference temperature, and $\tau_{ij} \overset{\text{def}}{=} \overline{u_i u_j} - \bar{u}_i\bar{u}_j$ and $h_j \overset{\text{def}}{=} \overline{u_j\theta} - \bar{u}_j\bar{\theta}$ are the SGS stress tensor and HF vector, respectively. The appearance of τ_{ij} and h_j is due to the grid-level filtering process. They represent the SGS effects related to the resolved velocity and temperature fields and need to be modelled in order to close the above system of governing equations.

2.1. SGS stress model

In this paper, we investigate four SGS HF models. This research focuses on the SGS HF models, rather than the SGS stress models. Thus, in order to provide a common basis for a comparative study of different SGS HF models, we will use only one SGS stress model for closure of the filtered momentum equation; namely, the dynamic nonlinear SGS stress model (DNM) recently proposed by Wang and Bergstrom (2005). The DNM is based on an explicit nonlinear quadratic tensorial polynomial constitutive relation originally proposed by Speziale (1987) and Gatski and Speziale (1993) for modelling of the Reynolds stress tensor in the Reynolds-averaged Navier–Stokes (RANS) approach. By analogy, the SGS stress tensor can be modelled using the following functional form within the context of the LES approach, viz.

$$\tau^*_{ij} = -C_S\beta_{ij} - C_W\gamma_{ij} - C_N\eta_{ij}, \tag{4}$$

where an asterisk represents a trace-free tensor, i.e. $(\cdot)^*_{ij} \overset{\text{def}}{=} (\cdot)_{ij} - (\cdot)_{kk}\delta_{ij}/3$, and the base tensor functions are defined as $\beta_{ij} \overset{\text{def}}{=} 2\overline{\Delta}^2|\overline{S}|\overline{S}_{ij}$, $\gamma_{ij} \overset{\text{def}}{=} 4\overline{\Delta}^2(\overline{S}_{ik}\overline{\Omega}_{kj} + \overline{S}_{jk}\overline{\Omega}_{ki})$ and $\eta_{ij} \overset{\text{def}}{=} 4\overline{\Delta}^2(\overline{S}_{ik}\overline{S}_{kj} - \overline{S}_{mn}\overline{S}_{nm}\delta_{ij}/3)$. Here, $\overline{\Delta}$ is the grid-level filter width; δ_{ij} is the Kronecker delta; $\overline{S}_{ij} \overset{\text{def}}{=} (\partial\bar{u}_i/\partial x_j + \partial\bar{u}_j/\partial x_i)/2$ and $\overline{\Omega}_{ij} \overset{\text{def}}{=} (\partial\bar{u}_i/\partial x_j - \partial\bar{u}_j/\partial x_i)/2$ are the resolved strain and rotation rate tensors, respectively; and, $|\overline{S}| = (2\overline{S}_{ij}\overline{S}_{ij})^{1/2}$ is the norm of the resolved strain rate tensor. It can be shown (Wang and Bergstrom, 2005) that the values of the three model coefficients C_S, C_W and C_N can be obtained by minimizing the residual of the Germano identity following the dynamic procedure of Lilly (1992) as

$$\begin{bmatrix} M_{ij}M_{ij} & M_{ij}W_{ij} & M_{ij}N_{ij} \\ W_{ij}M_{ij} & W_{ij}W_{ij} & W_{ij}N_{ij} \\ N_{ij}M_{ij} & N_{ij}W_{ij} & N_{ij}N_{ij} \end{bmatrix} \cdot \begin{bmatrix} C_S \\ C_W \\ C_N \end{bmatrix} = - \begin{bmatrix} \mathscr{L}^*_{ij}M_{ij} \\ \mathscr{L}^*_{ij}W_{ij} \\ \mathscr{L}^*_{ij}N_{ij} \end{bmatrix}, \tag{5}$$

where $\mathscr{L}_{ij} \overset{\text{def}}{=} \widetilde{\bar{u}_i\bar{u}_j} - \tilde{\bar{u}}_i\tilde{\bar{u}}_j$ is the resolved Leonard type stress; $M_{ij} \overset{\text{def}}{=} \alpha_{ij} - \tilde{\beta}_{ij}$, $W_{ij} \overset{\text{def}}{=} \lambda_{ij} - \tilde{\gamma}_{ij}$ and $N_{ij} \overset{\text{def}}{=} \zeta_{ij} - \tilde{\eta}_{ij}$ are

differential tensors, respectively; and $\alpha_{ij} \stackrel{\text{def}}{=} 2\widetilde{\overline{\Delta}}^2|\widetilde{\overline{S}}|\widetilde{\overline{S}}_{ij}$, $\lambda_{ij} \stackrel{\text{def}}{=} 4\widetilde{\overline{\Delta}}^2(\widetilde{\overline{S}}_{ik}\widetilde{\overline{\Omega}}_{kj} + \widetilde{\overline{S}}_{jk}\widetilde{\overline{\Omega}}_{ki})$ and $\zeta_{ij} \stackrel{\text{def}}{=} 4\widetilde{\overline{\Delta}}^2(\widetilde{\overline{S}}_{ik}\widetilde{\overline{S}}_{kj} - \widetilde{\overline{S}}_{mn}\widetilde{\overline{S}}_{nm}\delta_{ij}/3)$. Here, quantities filtered at the grid-level are denoted using an overbar and those filtered at the test-grid-level are denoted using a tilde.

The design of the constitutive relation of Eq. (4), in terms of the choice of the three constituent tensorial base components (i.e., β_{ij}, γ_{ij} and η_{ij}) is not arbitrary: (i) the first term β_{ij} is the well-known Smagorinsky component which primarily relates to the SGS dissipation and forward scatter of turbulence kinetic energy (TKE) from the resolved to subgrid scale motions; (ii) the second term γ_{ij} does not make any contribution to the TKE transfer between the resolved and subgrid scales, but according to a recent systematic *a priori* LES study of Horiuti (2003), it significantly improves the correlation between the exact τ_{ij} extracted from a DNS database and that predicted by the nonlinear model; and (iii) as demonstrated previously (Wang and Bergstrom, 2005), the third term η_{ij} contributes significantly to the backscatter of TKE from the subgrid to the resolved scales. The three features mentioned above, namely, an adequate SGS dissipation level, a high correlation coefficient between the modelled and exact SGS stress in an *a priori* LES test, and a realistic representation of TKE backscatter, are among the most important criteria for evaluation of a successful SGS stress model. The Speziale constitutive relation on which the DNM is based, offers an effective representation for modelling these three important physical features separately using three linearly independent tensorial terms. Further investigation and application of the DNM can be found in, e.g. Wang et al. (2006a) as it relates to topological features of wall-bounded turbulent flows and Wang et al. (2006b) as it relates to geometrical properties of the SGS stress tensor.

2.2. SGS heat flux models

In this Subsection, we introduce four dynamic SGS HF models, all characterized by a constitutive relation that is a function of a second order symmetric tensor $\mathbf{M}$ (e.g., $\overline{S}_{ij}$) and vector $\mathbf{v}$ (e.g., $\partial\bar{\theta}/\partial x_j$), viz.

$$\mathbf{h} = f(\mathbf{M}, \mathbf{v}) \quad \text{or} \quad h_j = f(\overline{S}_{ij}, \partial\bar{\theta}/\partial x_j). \tag{6}$$

Within this context, we first review two important dynamic SGS HF models: the DEDM-HF and DHLTDM-HF. Then we propose two new dynamic SGS HF models; namely, the dynamic full (or inhomogeneous) linear tensor diffusivity model (DFLTDM-HF) and the complete and irreducible dynamic nonlinear tensor diffusivity model (DNTDM-HF). The relationship between these four dynamic SGS HF models will also be discussed.

2.2.1. Model 1 (DEDM-HF): dynamic eddy diffusivity model for the SGS heat flux

The DEDM-HF of Moin et al. (1991), Cabot (1992), Sullivan and Moeng (1992), and Wong and Lilly (1994) expresses the SGS heat flux as

$$h_j = -C_{\theta E}\overline{\Delta}^2|\overline{S}|\frac{\partial\bar{\theta}}{\partial x_j}, \tag{7}$$

where the scalar eddy diffusivity embodied in Eq. (7) is $\alpha_{\text{sgs}} = C_{\theta E}\overline{\Delta}^2|\overline{S}|$, which can be further written in a general tensor diffusivity form using the Kronecker delta as

$$D^E_{jk} = \alpha_{\text{sgs}}\delta_{jk} = C_{\theta E}\overline{\Delta}^2|\overline{S}|\delta_{jk}. \tag{8}$$

With this notion, Eq. (7) can be simplified to $h_j = -D^E_{jk}\frac{\partial\bar{\theta}}{\partial x_k}$. Introducing the grid-level and test-grid-level base vector functions as: $b^E_j \stackrel{\text{def}}{=} \overline{\Delta}^2|\overline{S}|\frac{\partial\bar{\theta}}{\partial x_j}$ and $a^E_j \stackrel{\text{def}}{=} \widetilde{\overline{\Delta}}^2|\widetilde{\overline{S}}|\frac{\partial\widetilde{\bar{\theta}}}{\partial x_j}$, the SGS HF vector at the grid-level as represented by Eq. (7) can then be expressed as $h_j = -C_{\theta E}b^E_j$. Similarly, the SGS HF vector at the test-grid-level ($H_j \stackrel{\text{def}}{=} \widetilde{\overline{u_j\theta}} - \tilde{\bar{u}}_j\tilde{\bar{\theta}}$) can be modelled as $H_j = -C_{\theta E}a^E_j$. The grid- and test-grid-level SGS HF vectors satisfy the *vector identity*:

$$\mathscr{L}_j = H_j - \tilde{h}_j, \tag{9}$$

where $\mathscr{L}_j \stackrel{\text{def}}{=} \widetilde{\overline{u}_j\bar{\theta}} - \tilde{\bar{u}}_j\tilde{\bar{\theta}}$ and is directly computable at the resolved scale. By substituting the grid- and test-grid-level SGS HF models into the vector identity and assuming that $\tilde{h}_j = -\widetilde{C_{\theta E}b^E_j} \approx -C_{\theta E}\tilde{b}^E_j$, a residual vector that accounts for the difference between the left-hand-side (LHS) and right-hand-side (RHS) of the vector identity emerges:

$$\mathscr{E}_j = \mathscr{L}_j + C_{\theta E}(a^E_j - \tilde{b}^E_j) = \mathscr{L}_j + C_{\theta E}P_j, \tag{10}$$

where $P_j \stackrel{\text{def}}{=} a^E_j - \tilde{b}^E_j$ is a differential vector. By minimizing the norm of the residual vector (i.e., $\mathscr{E} \stackrel{\text{def}}{=} \mathscr{E}_j\mathscr{E}_j$) using the least squares method, the model coefficient $C_{\theta E}$ can be obtained as

$$C_{\theta E} = -\frac{\mathscr{L}_jP_j}{P_jP_j}. \tag{11}$$

2.2.2. Model 2 (DHLTDM-HF): dynamic homogeneous linear tensor diffusivity model for the SGS heat flux

The DHLTDM-HF proposed by Peng and Davidson (2002) for study of buoyancy driven flows assumes the following form:

$$h_j = -D^{\text{HL}}_{jk}\frac{\partial\bar{\theta}}{\partial x_k} = -C_{\theta S}\overline{\Delta}^2\overline{S}_{jk}\frac{\partial\bar{\theta}}{\partial x_k}, \tag{12}$$

where the tensor diffusivity is a homogeneous linear tensor function of $\overline{S}_{ij}$, viz.

$$D^{\text{HL}}_{jk} = f(\overline{S}_{jk}) = C_{\theta S}\overline{\Delta}^2\overline{S}_{jk}. \tag{13}$$

Here, *homogeneity* derives from the terminology of linear algebra for which a linear transformation that verifies: $D^{\text{HL}}_{jk} = f(\overline{S}_{jk}) = \mathbf{0}$ if $\overline{S}_{jk} = \mathbf{0}$ is referred to as being homogeneous. Following a similar dynamic procedure, the grid- and test-grid-level SGS HF vectors can be expressed as $h_j = -C_{\theta S}b^S_j$ and $H_j = -C_{\theta S}a^S_j$, respectively. On assuming $\widetilde{C_{\theta S}b^S_j} \approx C_{\theta S}\tilde{b}^S_j$, the model coefficient can be optimized using the least squares method as

$$C_{\theta S} = -\frac{\mathscr{L}_j Q_j}{Q_j Q_j}. \tag{14}$$

Here, $b_j^S \overset{\text{def}}{=} \overline{\Delta}^2 \overline{S}_{jk} \frac{\partial \bar{\theta}}{\partial x_k}$ and $a_j^S \overset{\text{def}}{=} \widetilde{\overline{\Delta}}^2 \widetilde{\overline{S}}_{jk} \frac{\partial \tilde{\bar{\theta}}}{\partial x_k}$ are the base vector functions, and $Q_j \overset{\text{def}}{=} a_j^S - \tilde{b}_j^S$ is a differential vector.

2.2.3. Model 3 (DFLTDM-HF): dynamic full linear tensor diffusivity model for the SGS heat flux

The tensor diffusivity for the DEDM-HF is a function of $\overline{S}_{ij}$ of the zeroth order (i.e., $D_{jk}^E = C_{\theta E}\overline{\Delta}^2|\overline{S}|\delta_{jk}$), and the tensor diffusivity for the DHLTDM-HF is a homogeneous linear function of $\overline{S}_{ij}$ of the first order (i.e., $D_{jk}^{\text{HL}} = C_{\theta S}\overline{\Delta}^2\overline{S}_{jk}$). According to the theory of tensor polynomial functions, a full linear tensor diffusivity function of $\overline{S}_{jk}$ includes both these two special cases, viz.

$$D_{jk}^{\text{FL}} = D_{jk}^E + D_{jk}^{\text{HL}} = C_{\theta E}\overline{\Delta}^2|\overline{S}|\delta_{jk} + C_{\theta S}\overline{\Delta}^2\overline{S}_{jk}, \tag{15}$$

which corresponds to the following constitutive relation for our proposed *dynamic full linear tensor diffusivity model for representing the SGS heat flux* (DFLTDM-HF):

$$h_j = -D_{jk}^{\text{FL}}\frac{\partial\bar{\theta}}{\partial x_k} = -C_{\theta E}\overline{\Delta}^2|\overline{S}|\frac{\partial\bar{\theta}}{\partial x_j} - C_{\theta S}\overline{\Delta}^2\overline{S}_{jk}\frac{\partial\bar{\theta}}{\partial x_k}. \tag{16}$$

Using the base vector functions defined above, the grid- and test-grid-level SGS HF vectors can be expressed as $h_j = -C_{\theta E}b_j^E - C_{\theta S}b_j^S$ and $H_j = -C_{\theta E}a_j^E - C_{\theta S}a_j^S$, respectively. The dynamic model coefficients $C_{\theta E}$ and $C_{\theta S}$ can be obtained by minimizing the residual ($\mathscr{E}$) of the vector identity using the least squares method. It can be shown that by setting $\partial\mathscr{E}/\partial C_{\theta E} = 0$ and $\partial\mathscr{E}/\partial C_{\theta S} = 0$, the following system of equations for computing the model coefficients is obtained:

$$\begin{bmatrix} P_jP_j & P_jQ_j \\ Q_jP_j & Q_jQ_j \end{bmatrix} \cdot \begin{bmatrix} C_{\theta E} \\ C_{\theta S} \end{bmatrix} = -\begin{bmatrix} \mathscr{L}_jP_j \\ \mathscr{L}_jQ_j \end{bmatrix}. \tag{17}$$

2.2.4. Model 4 (DNTDM-HF): complete and irreducible dynamic nonlinear tensor diffusivity model for the SGS heat flux

According to the theory of tensor invariants and functions, a vector-valued function of a second-order symmetric tensor $\mathbf{M}$ and a vector $\mathbf{v}$ can be represented by Noll's formula (Zheng, 1994) as follows:

$$\mathbf{h} = \varphi_0\mathbf{v} + \varphi_1\mathbf{M}\mathbf{v} + \varphi_2\mathbf{M}^2\mathbf{v}, \tag{18}$$

where $\varphi_i\,(i = 0, 1, 2)$ are coefficients of the form $\varphi_i = \varphi_i(I_M, II_M, III_M, I_v, I_{Mv}, II_{Mv})$. Here, $I_M = \text{tr}(\mathbf{M})$, $II_M = \text{tr}(\mathbf{M}^2)$ and $III_M = \text{tr}(\mathbf{M}^3)$ are the three independent invariants of $\mathbf{M}$; $I_v = \mathbf{v}\cdot\mathbf{v}$ is the invariant of $\mathbf{v}$; and $I_{Mv} = \mathbf{v}\cdot\mathbf{M}\mathbf{v}$ and $II_{Mv} = \mathbf{v}\cdot\mathbf{M}^2\mathbf{v}$ are the two independent invariants for $\mathbf{M}$ and $\mathbf{v}$. Noll's formula provides the complete and irreducible tensor function of $\mathbf{M}$ and $\mathbf{v}$, forming the basis for our proposed *complete and irreducible dynamic nonlinear tensor diffusivity model for representing the SGS heat flux* (DNTDM-HF):

$$\begin{aligned} h_j &= -D_{jk}^N\frac{\partial\bar{\theta}}{\partial x_k} \\ &= -C_{\theta E}\overline{\Delta}^2|\overline{S}|\frac{\partial\bar{\theta}}{\partial x_j} - C_{\theta S}\overline{\Delta}^2\overline{S}_{jk}\frac{\partial\bar{\theta}}{\partial x_k} - C_{\theta N}\overline{\Delta}^2\frac{\overline{S}_{ji}\overline{S}_{ik}}{|\overline{S}|}\frac{\partial\bar{\theta}}{\partial x_k}, \end{aligned} \tag{19}$$

where the tensor diffusivity is a quadratic nonlinear tensor function of $\overline{S}_{ij}$, viz.

$$D_{jk}^N = C_{\theta E}\overline{\Delta}^2|\overline{S}|\delta_{jk} + C_{\theta S}\overline{\Delta}^2\overline{S}_{jk} + C_{\theta N}\overline{\Delta}^2\frac{\overline{S}_{ji}\overline{S}_{ik}}{|\overline{S}|}. \tag{20}$$

Eqs. (18) and (19) are *inhomogeneous* due to the presence of the SGS eddy diffusivity term (the term related to δ_{jk}), *irreducible* because none of $\mathbf{v}$, $\mathbf{M}\mathbf{v}$ and $\mathbf{M}^2\mathbf{v}$ can be expressed as a single-valued function of the remaining terms, and *complete* because any vector function $\mathbf{h}$ of the form (6) can be expressed by (18). As such, no higher-order terms (e.g., a term related to $\overline{S}_{ji}\overline{S}_{il}\overline{S}_{lk}\cdot\partial\bar{\theta}/\partial x_k$) should appear in Eq. (19), because they cannot be independent of the existing terms. The denominator $|\overline{S}|$ appearing in the quadratic term in Eqs. (19) and (20) is required for dimensional consistency. Owing to the self-calibration mechanism of the dynamic procedure, other strategies (such as a time- and plane-averaged value, $\langle|\overline{S}|\rangle$) can be optionally considered as a replacement for the denominator should the need ever arise (e.g., to provide a tighter control on numerical stability for simulation of some specific flows).

Introducing the base vector functions: $b_j^N = \overline{\Delta}^2\frac{\overline{S}_{ji}\overline{S}_{ik}}{|\overline{S}|}\frac{\partial\bar{\theta}}{\partial x_k}$ and $a_j^N = \widetilde{\overline{\Delta}}^2\frac{\widetilde{\overline{S}}_{ji}\widetilde{\overline{S}}_{ik}}{|\widetilde{\overline{S}}|}\frac{\partial\tilde{\bar{\theta}}}{\partial x_k}$, the grid-level SGS heat flux [cf. Eq. (19)] can be simplified as

$$h_j = -C_{\theta E}b_j^E - C_{\theta S}b_j^S - C_{\theta N}b_j^N; \tag{21}$$

and similarly, the constitutive relation for the SGS heat flux at the test-grid-level can be expressed as

$$H_j = -C_{\theta E}a_j^E - C_{\theta S}a_j^S - C_{\theta N}a_j^N. \tag{22}$$

By substituting Eqs. (21) and (22) into the vector identity [i.e., Eq. (9)], a 3×3 matrix system for computing the model coefficients is obtained as follows:

$$[P_j, Q_j, R_j]\cdot[C_{\theta E}, C_{\theta S}, C_{\theta N}]^{\text{T}} = -\mathscr{L}_j, \tag{23}$$

for $j = 1$, 2 and 3. For brevity, we use $\mathbf{K}\cdot\mathbf{c} = -\mathbf{l}$ to denote the above linear system of equations. Here, $R_j \overset{\text{def}}{=} a_j^N - \tilde{b}_j^N$ is a differential vector. In our derivation of Eq. (23), we made use of an assumption analogous to that adopted in the dynamic procedure of Lilly (1992), viz. $\widetilde{C_{\theta E}b_j^E} \approx C_{\theta E}\tilde{b}_j^E$, $\widetilde{C_{\theta S}b_j^S} \approx C_{\theta S}\tilde{b}_j^S$ and $\widetilde{C_{\theta N}b_j^N} \approx C_{\theta N}\tilde{b}_j^N$. It should be pointed out that Eq. (23) is directly based on the vector identity [i.e., Eq. (9)] without invoking the least-squares approach. Because a vector involves three degrees of freedom, it is advantageous to build a SGS HF model with three dynamic coefficients such that the vector identity can be directly used for computing the model coefficients.

By left-multiplying both sides of Eq. (23) with $\mathbf{K}^{\text{T}}$, we obtain the following optional matrix system for computing the model coefficients:

$$(\mathbf{K}^{\mathrm{T}}\mathbf{K})\cdot\mathbf{c} = -\mathbf{K}^{\mathrm{T}}\cdot\mathbf{l} \tag{24}$$

or

$$\begin{bmatrix} P_jP_j & P_jQ_j & P_jR_j \\ Q_jP_j & Q_jQ_j & Q_jR_j \\ R_jP_j & R_jQ_j & R_jR_j \end{bmatrix}\cdot\begin{bmatrix} C_{\theta E} \\ C_{\theta S} \\ C_{\theta N} \end{bmatrix} = -\begin{bmatrix} P_j\mathscr{L}_j \\ Q_j\mathscr{L}_j \\ R_j\mathscr{L}_j \end{bmatrix}, \tag{24'}$$

which can be used as an alternative for computing the model coefficients. Eq. (24) can be also obtained using the least squares approach by setting $\partial\mathscr{E}/\partial C_{\theta E} = \partial\mathscr{E}/\partial C_{\theta S} = \partial\mathscr{E}/\partial C_{\theta N} = 0$, where $\mathscr{E} = \mathscr{E}_j\mathscr{E}_j$ and the residual vector $\mathscr{E}_j$ takes the following form in this specific case:

$$\begin{aligned}\mathscr{E}_j &= \mathscr{L}_j + C_{\theta E}(a_j^E - \tilde{b}_j^E) + C_{\theta S}(a_j^S - \tilde{b}_j^S) \\ &\quad + C_{\theta N}(a_j^N - \tilde{b}_j^N) = \mathscr{L}_j + C_{\theta E}P_j + C_{\theta S}Q_j + C_{\theta N}R_j.\end{aligned} \tag{25}$$

Because $\delta_{jk}\frac{\partial\bar{\theta}}{\partial x_k}$, $\overline{S}_{jk}\frac{\partial\bar{\theta}}{\partial x_k}$ and $\frac{\overline{S}_{ji}\overline{S}_{ik}}{|\overline{S}|}\frac{\partial\bar{\theta}}{\partial x_k}$ are linearly independent, P_j, Q_j and R_j are linearly independent. Therefore, the solution of either Eqs. (23) or (24) for the three model coefficients of the DNTDM-HF exists locally for an instantaneous thermal-fluid field. However, use of Eq. (24) [or Eq. (24′)] is computationally more expensive than use of Eq. (23) due to a few additional matrix operations. In this study, we use Eq. (23) to compute the three model coefficients. We observe in the numerical tests that both the proposed models, i.e. DFLTDM-HF [cf. Eq. (17)] and DNTDM-HF [cf. Eq. (23)] can be applied locally at each time step without resorting to a plane averaging technique for stable computation of the local model coefficients.

2.3. Relations between different SGS HF models

In Section 2.2, we have reviewed two conventional SGS HF models (i.e., the DEDM-HF and DHLTDM-HF), and also proposed two new models (i.e., the DFLTDM-HF and DNTDM-HF). In order to obtain a more comprehensive understanding of the proposed modelling approaches, it is important to compare the constitutive relations of these four models. The DNTDM-HF, which is directly derived from Noll's formula, represents the most general explicit expression for all the constitutive relations of the form of Eq. (6). The constitutive relation of the DNTDM-HF is explicit, complete, irreducible, nonlinear and inhomogeneous. If $C_{\theta N} = 0$, the quadratic term vanishes and the DNTDM-HF reduces to the DFLTDM-HF. Furthermore, the DFLTDM-HF reduces to the DHLTDM-HF if $C_{\theta E} = 0$ and to the DEDM-HF if $C_{\theta S} = 0$.

A 3D vector is uniquely determined by three degrees of freedom. Because the DNTDM-HF is based on three independent constituent tensorial terms [cf., Eq. (19)], the associated three model coefficients can be obtained exactly by directly solving the vector identity [cf., Eq. (23)]. In contrast, because only two independent constituent tensorial terms are present in the DFLTDM-HF, and only one constituent tensorial term is present in the DHLTDM-HF and DEDM-HF, the system of equations used to determine the model coefficient(s) for the latter three models (derived from the vector identity) is over-determined. Consequently, an exact solution of the model coefficient(s) is not available, and the least squares approach needs to be used to obtain the optimal value(s) of the model coefficient(s) for the DFLTDM-HF, DHLTDM-HF and DEDM-HF.

3. Test case and numerical algorithm

In order to validate the proposed SGS HF models, numerical simulations have been performed based on a combined (or mixed) forced and natural convective flow in a vertical channel following the test case of Kasagi and Nishimura (1997), who investigated the flow and temperature fields using DNS. Modern research on combined forced and natural turbulent convection was initiated in the 1960s based on various experimental investigations (see Metais and Eckert, 1964). Since then, refined experimental measurements have become available (Easby, 1978; Nakajima et al., 1980), and the research methodology has been extended to include numerical simulations based on the RANS (Abdelmeguid and Spalding, 1979; Tanaka et al., 1987) and DNS (Kasagi and Nishimura, 1997; Davidson et al., 2003) approaches. A detailed review of the subject (up to 1989) can be found in Jackson et al. (1989). Recently, LES has been utilized to investigate this type of flow, such as the work of Lee et al. (2004) who studied a heated flow in a vertical annular pipe, Zhang and Chen (2000) who studied indoor air flow, Yan (2003) who studied thermal plumes for different initial conditions, Tyagi and Acharya (2005) who studied heat transfer in a rotating channel flow with rib turbulators, Qin and Pletcher (2006) who systematically investigated turbulent heat transfer in a rotating square duct, and Wang et al. (2006c, 2007) who studied mixed convection in a vertical channel.

The computational domain used in our numerical simulations is $L_1 \times L_2 \times L_3 = 3\pi\delta \times 2\delta \times \pi\delta$. A coarse grid of $48 \times 32 \times 48$ nodes has been used for discretization of the computational domain in the streamwise (x_1), wall-normal (x_2) and spanwise (x_3) directions, respectively. Here, δ is the half channel width set to 40 mm. The geometry of the computational domain is shown in Fig. 1. The grid is uniform in the streamwise and spanwise directions, and is refined within the near-wall region in the wall-normal direction. No-slip and no-penetration boundary conditions were imposed on the velocity components at the walls, while the temperatures on the two side walls were set to fixed values derived from the given Grashof number. Periodic boundary conditions were imposed in the streamwise and spanwise directions. The flow is characterized by a Grashof number of $Gr = 9.6 \times 10^5$ and a Reynolds number of $Re_\tau^{\mathrm{a}} = 150$. The Grashof and Reynolds numbers are defined as $Gr = g\beta\Delta\theta(2\delta)^3/\nu^2$ and $Re_\tau = u_\tau\delta/\nu$, respectively, where u_τ is the wall friction velocity, and $\Delta\theta = \theta_{\mathrm{wh}} - \theta_{\mathrm{wc}}$ is the temperature difference between the hot and cold walls. Here, the superscript "a" denotes a value averaged over the

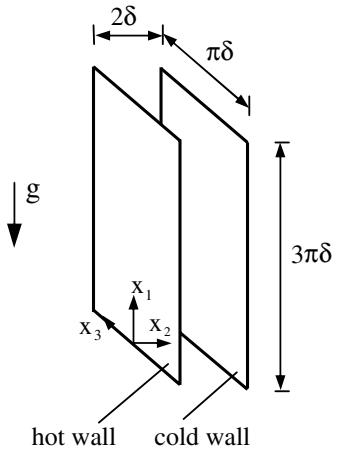

Fig. 1. Physical domain for the combined forced and natural convective flow.

hot and cold walls, so $Re_\tau^a = (Re_{\tau h} + Re_{\tau c})/2 = u_\tau^a \delta/v$. Because the velocity profile is asymmetric in the wall-normal direction, the value of the friction velocity τ_w (and therefore, the Reynolds number Re_τ) at the hot wall is different than that at cold wall, i.e. $\tau_{wh} \neq \tau_{wc}$ (and $Re_{\tau h} \neq Re_{\tau c}$).

The governing equations are discretized using the finite volume method. Following the approach of Kim and Moin (1985), the momentum equations were solved using a fractional-step method where the nonlinear term was discretized using a second-order explicit Adams–Bashforth scheme and the viscous diffusion term was discretized using a second-order Crank–Nicolson scheme. A second-order central difference scheme was applied on a collocated grid for spatial discretization. At each time step, the pressure field was updated using an pressure correction method and the Poisson type pressure correction equation was solved using a multigrid method. The checkerboard effect in the pressure field associated with the adopted collocated grid system was removed using a momentum interpolation scheme for evaluating the velocity at the faces of the control volumes (Rhie and Chow, 1983). To solve the thermal energy equation, a fourth-order Runge–Kutta method was used to advance the temperature field over a single time step. The turbulent flow and temperature statistics reported here were based on an average over 30,000 time steps after the flow becomes fully developed. In presentation of the results, all quantities denoted by $\langle \cdot \rangle$ correspond to averages both in time and over the homogeneous x_1–x_3 plane; and quantities non-dimensionalized using the friction velocity u_τ and friction temperature $T_\tau \stackrel{\text{def}}{=} q_w/(\rho c_P u_\tau)$ are denoted with a superscript "+". Here, q_w represents the wall heat flux and c_P is the specific heat at constant pressure. In order to make use of the DNS data of Kasagi and Nishimura (1997) in our comparative analysis, we follow their convention for normalizing flow quantities in the wall coordinate system and use $u_{\tau h}$ and $T_{\tau h}$ for the hot wall region (or the aiding flow region) and $u_{\tau c}$ and $T_{\tau c}$ for the cold wall region (or the opposing flow region).

4. Numerical results

In order to validate the numerical results, two sets of DNS data of Kasagi and Nishimura (1997) (denoted as KN-1997) are used for comparison; namely, one set of DNS data for mixed convective flow ($Gr = 9.6 \times 10^5$ and $Re_\tau^a = 150$) and one for forced convective flow where temperature evolves as a passive scalar ($Re_\tau = 150$ with no buoyancy term appearing in the filtered momentum equation). The DNS results for the purely forced convection case ($Gr = 0$ and $Re_\tau = 150$) conducted by Kuroda et al. (1995) (denoted as KKN-1995) are also used in our comparative study.

4.1. Mean resolved velocity and temperature fields

Figs. 2a and b show the profiles of the mean resolved streamwise velocity and temperature across the channel. The mean velocity and temperature profiles are symmetric for forced convection, whereas they are asymmetric for the mixed convection case. The results predicted by the four SGS HF models are consistent and agree in general with the DNS data, except for some small differences. In comparison with the DNS results, the mean temperature is slightly underpredicted near the hot wall. Figs. 3a and b show the predicted mean streamwise velocity and temperature profiles using wall coordinates. In comparison with the purely forced convection case, the velocity profile for the aiding flow deforms and a logarithmic region no longer exists near the hot wall; while near the cold wall, the velocity profile for the opposing flow shifts downwards. The mean temperature profile also strongly responds to the buoyant force, shifting upwards and downwards near the hot and cold walls, respectively. As expected, from Figs. 2 and 3, it is observed that the performance of the four tested SGS HF models is similar and they all can successfully predict the wall-normal distribution of the mean streamwise velocity and temperature at the resolved scale. This is not surprising, since in LES, large resolved scale motions are directly computed, temporally and spatially.

Figs. 4, 5 show the predicted resolved velocity and temperature fluctuations [or root-mean-square (RMS) values], which are defined as $\bar{u}_{i,\text{rms}}^+ \stackrel{\text{def}}{=} \langle (\frac{\bar{u}_i - \langle \bar{u}_i \rangle}{u_\tau})^2 \rangle^{1/2}$ for $i = 1$, 2 and 3, and $\bar{\theta}_{\text{rms}}^+ \stackrel{\text{def}}{=} \langle (\frac{\bar{\theta} - \langle \bar{\theta} \rangle}{T_\tau})^2 \rangle^{1/2}$, respectively. From Figs. 4a–c, it is observed that in comparison with the DNS results, the level of all three velocity fluctuation components $\bar{u}_{i,\text{rms}}^+$ for both the aiding and opposing flows is slightly underpredicted. On the aiding side, it can be seen in Figs. 4a–c that the prediction from the DNTDM-HF is, in general, in better conformance with the DNS data than the other three SGS HF models. Characteristic to this flow, the effect of buoyancy is to enhance the level of all three velocity fluctuation components in the opposing flow and to reduce their levels in the aiding flow. In contrast, it is observed from Fig. 5 that buoyancy increases the temperature fluctuation level $\bar{\theta}_{\text{rms}}^+$ in the aiding flow and decreases it in the opposing flow.

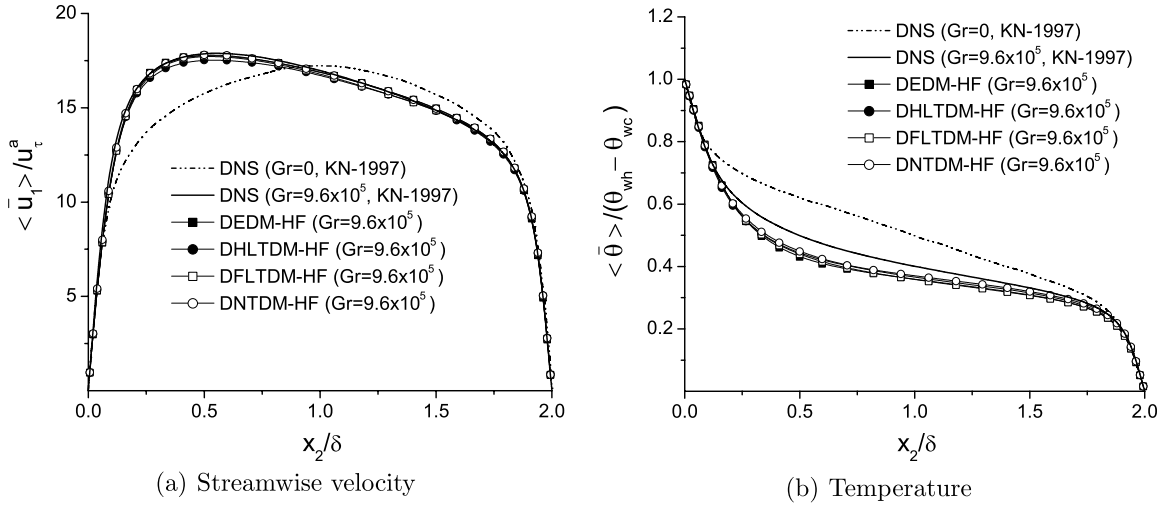

Fig. 2. Profiles of the mean resolved velocity and temperature fields in the wall-normal direction.

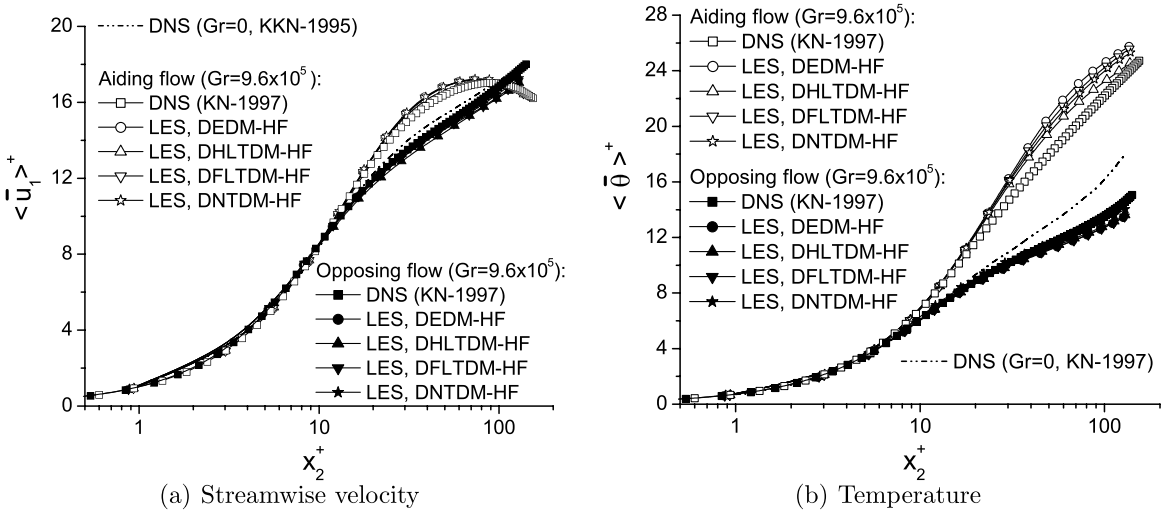

Fig. 3. Profiles of the mean resolved velocity and temperature displayed using wall coordinates.

Although slight differences are observed between different models in terms of their predictions of $\bar{u}^{+}_{i,\mathrm{rms}}$ and $\bar{\theta}^{+}_{\mathrm{rms}}$, the differences are in general insignificant. As discussed previously, this is because both $\bar{u}^{+}_{i,\mathrm{rms}}$ and $\bar{\theta}^{+}_{\mathrm{rms}}$ are resolved quantities extracted at the filtered level, and with a reasonable SGS modelling and grid resolution, an LES approach should be successful in predicting their values. The reason that the turbulent intensities are underpredicted is due to the fact that for an LES approach which uses trace-free SGS stress models, only the deviatoric part of the time- and plane-averaged exact Reynolds stress tensor (as extracted from the DNS data) can be approximately reproduced (Winckelmans et al., 2002; Sagaut, 2002), viz. $\langle \bar{u}_i'' \bar{u}_j'' \rangle + \langle \tau_{ij} \rangle$. Because the value of $\langle \tau_{ii} \rangle$ (no summation convention is implied here) is not available, exact turbulent intensities associated with the diagonal components of the Reynolds stress tensor cannot be fully recovered.

Figs. 6 and 7 show the time- and plane-averaged model coefficients for the SGS stress model DNM and SGS HF model DNTDM-HF, respectively. Due to the existence of buoyancy, the dynamic coefficients for both models are asymmetrical about $x_2/\delta = 1$. Although the value of $|C_S|$ is smaller than those of $|C_W|$ and $|C_N|$, the difference between these values is less than one order of magnitude, implying that all the three independent tensorial terms shown in Eq. (4) for the DNM are important for this specific flow. As shown in Fig. 7, a similar conclusion holds for the DNTDM-HF based on comparing the relative magnitudes of the three model coefficients $C_{\theta E}$, $C_{\theta S}$ and $C_{\theta N}$.

4.2. Budgets of shear stresses and heat fluxes

In order to investigate the performance of the proposed DFLTDM-HF and DNTDM-HF in terms of their influence on the balance of momentum and thermal energy, we examine the budgets for shear stress and heat flux across the channel. An instantaneous filtered quantity $\bar{\phi}$ can be decomposed into mean and residual components as

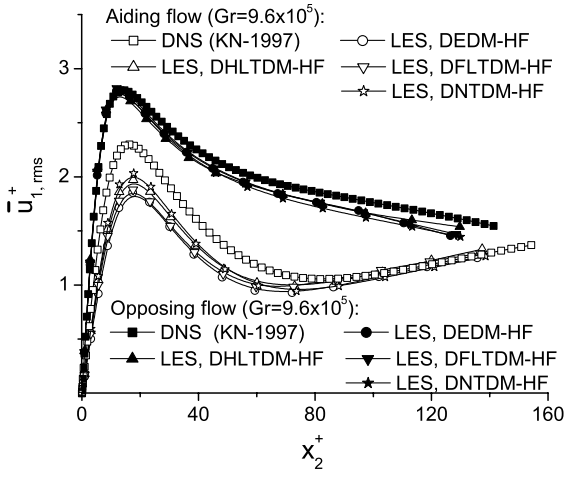

(a) RMS of the streamwise velocity

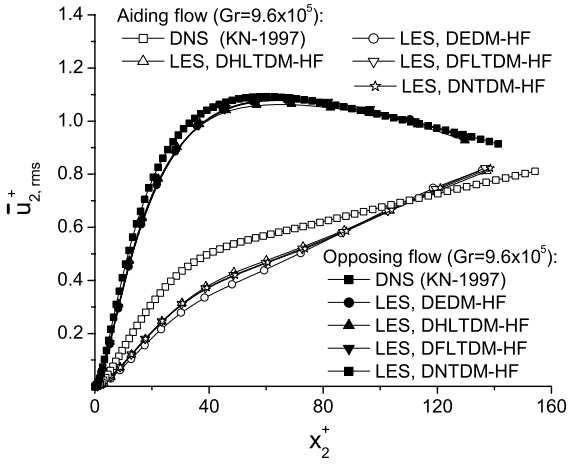

(b) RMS of the wall-normal velocity

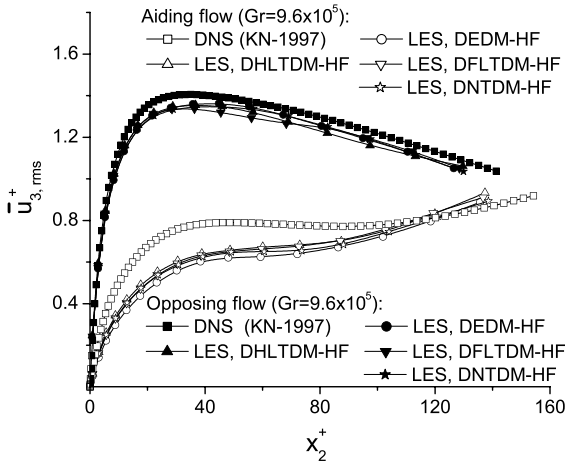

(c) RMS of the spanwise velocity

Fig. 4. Resolved velocity fluctuations displayed in wall coordinates.

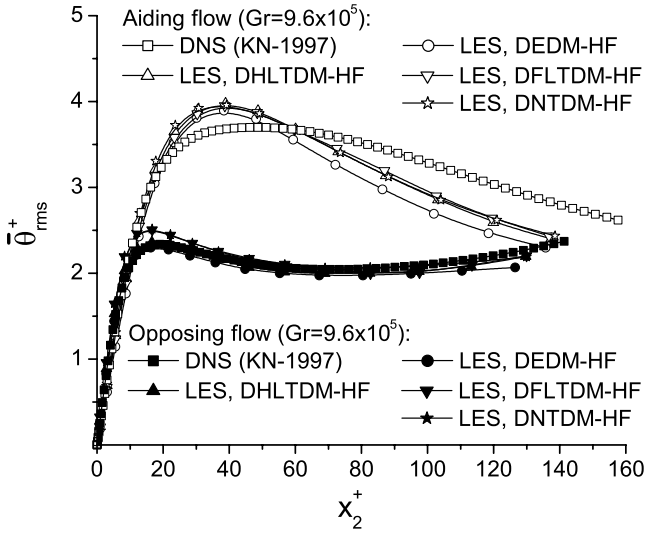

Fig. 5. Resolved temperature fluctuations displayed in wall coordinates.

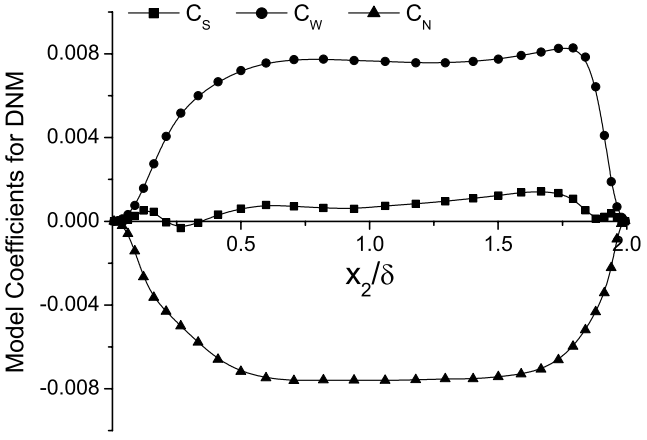

Fig. 6. Averaged model coefficients for the SGS stress model DNM.

$$\bar{\phi} = \langle\bar{\phi}\rangle + \bar{\phi}'', \tag{26}$$

where $\langle\bar{\phi}\rangle$ denotes a filtered quantity averaged both in time and over the homogeneous (x_1–x_3) plane, and $\bar{\phi}''$ denotes the residual component relative to $\langle\bar{\phi}\rangle$. By substituting Eq. (26) into the filtered streamwise momentum equation

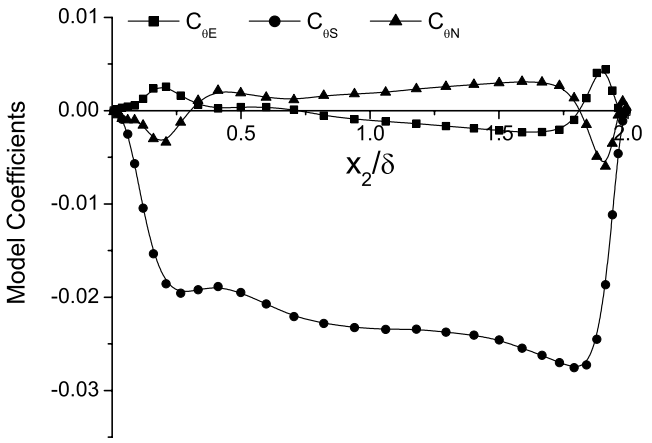

Fig. 7. Averaged model coefficients for the SGS HF model DNTDM-HF.

and then integrating the resulting equation from 0 to x_2 in the wall-normal direction, a budget equation for time- and plane-averaged shear stresses at an arbitrary wall-normal location x_2 is obtained:

$$\nu\frac{\partial\langle\bar{u}_1\rangle}{\partial x_2}-\langle\bar{u}_1''\bar{u}_2''\rangle+\int_0^{x_2}\beta g(\langle\bar{\theta}\rangle-\Theta_r)\,\mathrm{d}x_2-\langle\tau_{12}\rangle=\frac{1}{\rho}\frac{\partial\langle\bar{p}\rangle}{\partial x_1}x_2+\frac{\tau_{wh}}{\rho}. \tag{27}$$

In order to derive this equation, two additional assumptions were made: the flow is: (i) statistically stationary and (ii) homogeneous in the x_1–x_3 plane (so, $\langle\bar{u}_2\rangle=0$ and $\langle\bar{u}_2''\rangle=0$). The four terms on the LHS of Eq. (27) represent the resolved viscous shear stress (RVSS), resolved Reynolds (or turbulent) shear stress (RTSS), resolved buoyant shear stress (RBSS), and SGS shear stress (SGS SS), respectively. The two terms on the RHS of the equation represent the resolved integrated driving force due to the mean pressure gradient, and the resolved viscous shear stress at the hot wall $\left(\tau_{wh}=\rho\nu\frac{\partial\langle\bar{u}_1\rangle}{\partial x_2}|_{x_2=0}\right)$, respectively. In order for Eq. (27) to balance at both wall surfaces, the reference temperature Θ_r is taken as the bulk temperature, viz. $\Theta_r=\theta_B=\int_0^{2\delta}\langle\bar{\theta}\rangle\,\mathrm{d}x_2/2\delta$. With this convention, the RBSS term in Eq. (27) vanishes at both wall surfaces.

Figs. 8a and b show the shear stress budget predicted using both the proposed DFLTDM-HF and DNTDM-HF, respectively. All the terms exhibited in these figures are non-dimensionalized using the viscous shear stress term averaged over the hot and cold walls [i.e., τ_w^a/ρ or $(u_\tau^a)^2$]. As evident from Fig. 8, the distribution of RTSS and RBSS is asymmetrical across the channel, owing to the effects of the buoyant force. Although two assumptions were made to derive Eq. (27) from the filtered momentum equation, the balance expressed by this equation is consistent with the results obtained from the numerical simulation. As evident in both Figs. 8a and b, the total shear stress calculated from the LHS of Eq. (27) agrees very well with that calculated from the RHS of the equation. Because the shear stresses shown in Fig. 8 are non-dimensionalized using $(u_\tau^a)^2$ [$u_\tau^a=(u_{\tau h}+u_{\tau c})/2$, and the value of $u_{\tau h}$ is different than that of $u_{\tau c}$ due to the existence of buoyancy], the predicted total shear stress slightly deviates from being exactly anti-symmetrical about $x_2/\delta=1$. As shown in Figs. 8a and b, the time- and plane-averaged SGS shear stress component $\langle-\tau_{12}\rangle$ is very small in comparison with the other shear stress components; however, the instantaneous value of the SGS shear stress $-\tau_{12}$ as indicated by dashed lines is significant at a specific location (e.g., along the central wall-normal line located at $x_1/L_1=x_3/L_3=0.49$).

Following a procedure similar to that used for deriving Eq. (27), the time- and plane-averaged equation expressing the balance of the mean wall-normal heat fluxes at any arbitrary wall-normal location x_2 can be obtained from the filtered energy Eq. (3):

$$-\alpha\frac{\partial\langle\bar{\theta}\rangle}{\partial x_2}+\langle\bar{u}_2''\bar{\theta}''\rangle+\langle h_2\rangle=\frac{q_{wh}}{\rho c_P}, \tag{28}$$

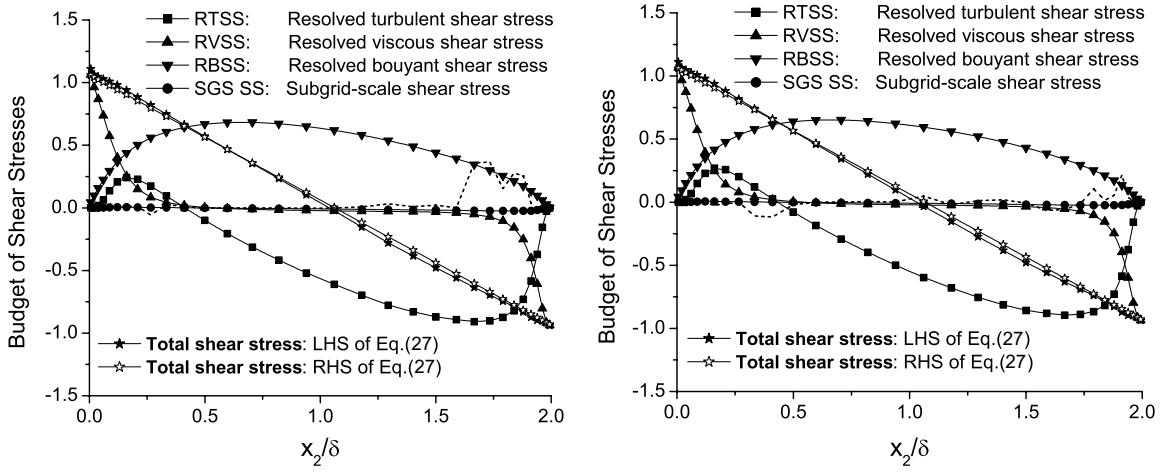

(a) DFLTDM-HF (b) DNTDM-HF

Fig. 8. Budget of shear stresses (non-dimensionalized using τ_w^a/ρ). Dashed lines: instantaneous wall-normal profile of the subgrid-scale shear stress $-\tau_{12}$ at the location $x_1/L_1=x_3/L_3=0.49$.

where $q_{wh} \overset{def}{=} -\lambda \frac{\partial \langle \bar{\theta} \rangle}{\partial x_2}|_{x_2=0}$ is the resolved molecular heat flux at the hot wall, and λ is the thermal conductivity. The three wall-normal HF components on the LHS of Eq. (28) correspond to the resolved molecular heat flux (RMHF), resolved turbulent heat flux (RTHF), and SGS heat flux (SGS HF), respectively. Fig. 9 plots the budget of the wall-normal heat flux terms exhibited in Eq. (28). All the terms shown in the figure are non-dimensionalized using the molecular heat flux at the hot wall, i.e. $q_{wh}/\rho c_P = u_{\tau h} T_{\tau h}$. With this normalization, the total heat flux given by the RHS of Eq. (28) becomes unity. As shown in Figs. 9a and b, both the proposed DFLTDM-HF and DNTDM-HF can provide a good balance of the wall-normal heat fluxes, since it is evident from the figures that these total heat flux calculated from the LHS of Eq. (28) agrees well with the theoretical value of 1.0. It should be noted that in Figs. 9a and b, the wall-normal SGS HF term (i.e., $\langle h_2 \rangle$) predicted by the two proposed models exhibits a different behaviour. The time- and plane-averaged value $\langle h_2 \rangle$ predicted by the DNTDM-HF becomes negative in the near-wall region, especially near the cold wall. In contrast, $\langle h_2 \rangle$ predicted by the DFLTDM-HF is positive across the entire channel. Also, as shown in Figs. 9a and b, in comparison with the time- and plane-averaged value $\langle h_2 \rangle$, the instantaneous value of the wall-normal SGS HF h_2 can exhibit relatively large fluctuations in amplitude locally (e.g., at the location $x_1/L_1 = x_3/L_3 = 0.49$).

As in the previous discussion, it can be shown that in this test case, the averaged true (exact) turbulent heat fluxes obtained from a DNS approach can be approximately recovered using the averaged resolved and SGS turbulent heat fluxes as $\langle \bar{u}_j'' \bar{\theta}'' \rangle + \langle h_j \rangle$. Figs. 10a and b show the streamwise and wall-normal turbulent heat fluxes (i.e., $\langle \bar{u}_1'' \bar{\theta}'' \rangle^+ + \langle h_1 \rangle^+$ and $\langle \bar{u}_2'' \bar{\theta}'' \rangle^+ + \langle h_2 \rangle^+$, respectively) using wall coordinates in comparison with the DNS data. From both Figs. 10a and b, it is observed that although slight

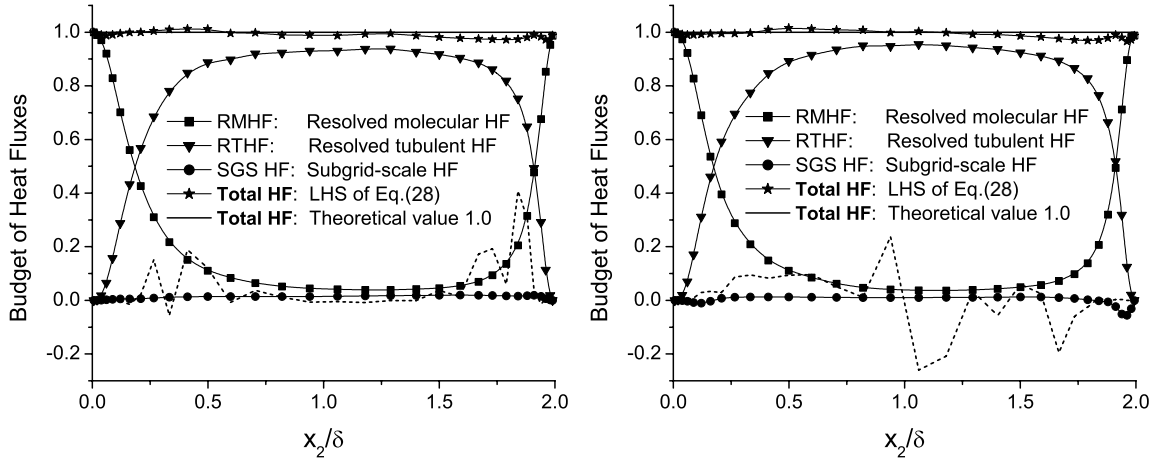

Fig. 9. Budget of heat fluxes in the wall-normal direction (non-dimensionalized using $q_{wh}/\rho c_P$). Dashed lines: instantaneous wall-normal profile of the subgrid-scale heat flux component h_2 at the location $x_1/L_1 = x_3/L_3 = 0.49$.

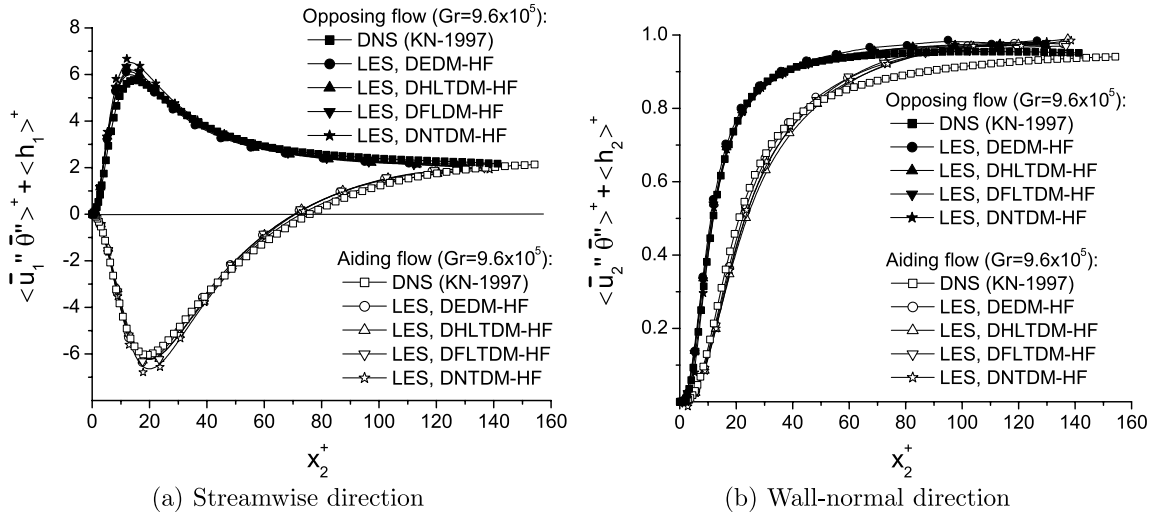

Fig. 10. Turbulent heat fluxes displayed using wall coordinates.

differences exist, the performance of the four tested SGS HF models are generally similar. All four tested models are capable of capturing the trend of the DNS profile, albeit the level of the wall-normal turbulent heat flux shown in Fig. 10b is slightly overpredicted by the simulation in the aiding flow region. The effect of buoyancy on the distribution of turbulent heat fluxes is evident in Fig. 10. Specifically, buoyancy enhances the level of the wall-normal turbulent heat flux in the opposing flow region and reduces it in the aiding flow region.

4.3. SGS effects

Until this point, we have primarily examined resolved quantities related to the velocity and temperature fields at the large filtered scale. Some SGS effects on the budgets of shear stresses and heat fluxes have also been briefly discussed. For instance, the highly fluctuating instantaneous local SGS shear stress $-\tau_{12}$ and SGS HF h_2 were compared with their time- and plane-averaged values in Figs. 8 and 9, respectively. In this Subsection, we continue investigating the SGS effects embodied in the SGS stress tensor τ_{ij} and SGS HF vector h_j. The discussion will focus on two tensor invariants; namely, the rate of local TKE flux P_r between the resolved and unresolved scales, and the characteristic alignment angle Φ between the SGS HF vector h_j and the resolved temperature gradient $\partial\bar{\theta}/\partial x_j$. The effective SGS thermal diffusivity predicted by four different SGS HF models will also be compared in order to highlight the SGS effects.

4.3.1. SGS effects on local energy flux

The rate of local TKE flux P_r between the resolved and unresolved scales is an invariant of τ^*_{ij} and $\overline{S}_{ij}$ through tensor contraction, viz.

$$P_r = -\tau^*_{ij}\overline{S}_{ij}, \tag{29}$$

which represents an inertial inviscid local energy flux between the resolved and unresolved subgrid scales. It represents the rate of TKE production and functions as a source of TKE for the residual SGS motions and a sink of TKE for the large resolved scale motions. The instantaneous value of P_r can be either positive or negative, representing a forward or backward TKE flux between the resolved and subgrid-scale motions, respectively. Fig. 11 shows the time- and plane-averaged value of P_r across the channel, non-dimensionalized using $(u^a_\tau)^4/\nu$. The forward scatter (i.e., $\langle P^+_r\rangle$) and backscatter (i.e., $\langle P^-_r\rangle$) of TKE have been separated, and these two quantities must verify: $\langle P_r\rangle = \langle P^+_r\rangle + \langle P^-_r\rangle$. From the figure, it is observed that the magnitude of $\langle P^+_r\rangle$ is much larger than that of $\langle P^-_r\rangle$, producing a net positive-valued $\langle P_r\rangle$ profile across the channel.

From Fig. 11, it is observed that the effect of buoyancy on the local energy flux is significant. In response to the buoyant force, the profiles of $\langle P_r\rangle$, $\langle P^+_r\rangle$ and $\langle P^-_r\rangle$ are asymmetric in the wall-normal direction across the channel, and

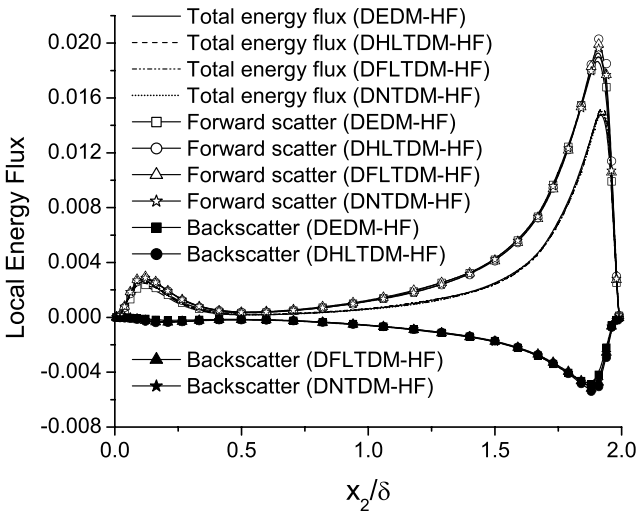

Fig. 11. Local energy flux between the filtered and subgrid scales [non-dimensionalized using $(u^a_\tau)^4/\nu$]. Forward scatter: $\langle P^+_r\rangle$; Backscatter: $\langle P^-_r\rangle$.

their level is much larger in the opposing flow than in the aiding flow, suggesting a stronger and more active local TKE transfer between the resolved and subgrid scales of motion in the cold wall region. By its very definition, P_r is directly determined by the SGS stress (τ_{ij}) which appears in the filtered momentum equation [cf. Eq. (2)], instead of the SGS heat flux (h_j) which appears in the filtered energy equation [cf. Eq. (3)]. From Eq. (3), it can be seen that the buoyancy term in the filtered momentum equation is determined directly from the resolved temperature field at the filtered scale, rather than any of the unresolved thermal quantities (such as the SGS HF h_j) at the subgrid scale. In consequence, although the buoyancy term plays a significant role in the filtered momentum Eq. (2), the effect of buoyancy on the momentum balance is due to the resolved temperature field (i.e., $\bar{\theta}$), which should not vary significantly from one SGS HF model to another (presuming that numerical simulations based on different models are all successful). This is not surprising because large-scale thermal variables (such as $\bar{\theta}$) are directly computed in an LES approach. Because the predictions of the resolved temperature field obtained from the four tested SGS HF models are similar [see Figs. 2b and 3b], and all four test cases for testing the SGS HF models are based on the same DNM for modelling the SGS stress, the differences in the predictions of $\langle P_r\rangle$ between the various test cases are expected to be small.

4.3.2. SGS effects on effective thermal diffusion

As mentioned earlier, the physical mechanism for the turbulent SGS HF transport process is fundamentally different than that for molecular heat conduction (or diffusion) governed by Fourier's law. Strictly speaking, the concept of molecular thermal diffusion cannot be used for describing the complex turbulent heat transfer process at the subgrid scale. For the DEDM-HF, because its constitutive relationship is based on an analogy to molecular

diffusion, the SGS eddy thermal diffusivity α_{sgs} can be explicitly defined through Eqs. (7) and (8). In contrast, the concept of a SGS eddy thermal diffusivity is not applicable for the DHLTDM-HF, DFLTDM-HF and DNTDM-HF. Rather, these three models rely on the physically more complex concept of a tensor thermal diffusivity: i.e., D_{jk}^{HL}, D_{jk}^{FL} and D_{jk}^{N} given by Eqs. (13), (15) and (20), respectively.

To compare the four SGS HF models in terms of the conventional concept of SGS eddy thermal diffusivity (which forms the basis of the classical DEDM-HF), it is useful to evaluate the *effective SGS thermal diffusivity* using the wall-normal SGS heat flux, viz. $\alpha_{sgs}^{e} \stackrel{def}{=} -h_2/(\partial\bar{\theta}/\partial x_2)$ for each of these models. Obviously, for the DEDM-HF, the effective SGS thermal diffusivity can be calculated explicitly from its definition, i.e. $\alpha_{sgs}^{e} \equiv \alpha_{sgs} \stackrel{def}{=} C_{\theta E}\overline{\Delta}^2|\bar{S}|$. In contrast, because the DHLTDM-HF, DFLTDM-HF and DNTDM-HF rely on the concept of a tensor diffusivity (D_{jk}), the effective SGS thermal diffusivity for these three models is evaluated as $\alpha_{sgs}^{e} = -D_{2k}(\partial\bar{\theta}/\partial x_k)/(\partial\bar{\theta}/\partial x_2)$. It is known that the performance of the DEDM-HF is very poor when the value of h_2 is finite (i.e., $h_2 \nrightarrow 0$) and the value of $|\partial\bar{\theta}/\partial x_2|$ is very small (i.e., $|\partial\bar{\theta}/\partial x_2| \to 0$), because the DEDM-HF by definition requires $h_2 \propto -\partial\bar{\theta}/\partial x_2 \to 0$. In contrast, in this situation, the DHLTDM-HF, DFLTDM-HF and DNTDM-HF have the potential to successfully predict a finite value of the wall-normal SGS HF h_2, owing to the involvement of the streamwise and spanwise temperature gradient components through a tensor contraction with D_{2k} [i.e., $h_2 = -D_{2k}(\partial\bar{\theta}/\partial x_k)$]. As such, it is anticipated that when the value of $|\partial\bar{\theta}/\partial x_2|$ is small, the amplitude of $|\alpha_{sgs}^{e}|$ predicted by the DEDM-HF is much smaller and less variable than those predicted by the DHLTDM-HF, DFLTDM-HF and DNTDM-HF.

Fig. 12 displays the time- and plane-averaged absolute value of the ratio of α_{sgs}^{e} and α (i.e., $\langle|\alpha_{sgs}^{e}/\alpha|\rangle$). The value for $\langle|\alpha_{sgs}^{e}/\alpha|\rangle$ predicted by the DEDM-HF ranges from 0 at the wall to approximately 0.45 at the center of the channel. In comparison, the values for $\langle|\alpha_{sgs}^{e}/\alpha|\rangle$ predicted by the DHLTDM-HF, DFLTDM-HF and DNTDM-HF vary from 0 at the wall to 12 at the center of the channel. This indicates that even in a time- and plane-averaged sense, the wall-normal SGS heat fluxes (which can be either positive or negative) predicted by the DHLTDM-HF, DFLTDM-HF and DNTDM-HF are much larger than those predicted by the DEDM-HF. Moreover, the wall-normal SGS heat flux predicted by DHLTDM-HF, DFLTDM-HF and DNTDM-HF are much larger than that due to molecular heat conduction at the center of the channel (because $\langle|\alpha_{sgs}^{e}/\alpha|\rangle > 1$). This further suggests that the classical concept of a scalar SGS eddy diffusivity inherent in the DEDM-HF is not a good assumption for use in modelling the SGS heat flux (at least at the subgrid scale).

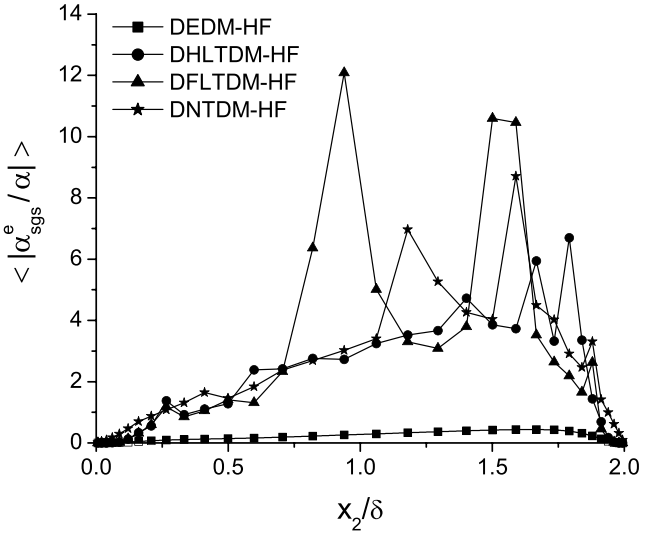

Fig. 12. Ratio of the effective SGS and molecular thermal diffusivities: $\langle|\alpha_{sgs}^{e}/\alpha|\rangle$.

It should be noted that the value of α_{sgs}^{e} for the DHLTDM-HF, DFLTDM-HF and DNTDM-HF discussed above is evaluated using the wall-normal heat flux h_2. It is possible to evaluate the value of α_{sgs}^{e} alternatively based on the streamwise heat flux h_1, viz. $\alpha_{sgs}^{e} \stackrel{def}{=} -h_1/(\partial\bar{\theta}/\partial x_1) = -D_{1k}(\partial\bar{\theta}/\partial x_k)/(\partial\bar{\theta}/\partial x_1)$. However, the spanwise SGS heat flux h_3 is not useful for this discussion, because of the periodicity and homogeneity of the flow and temperature fields and a lack of a mean convection and temperature gradient in the spanwise direction.

4.3.3. Geometrical characteristics of the SGS heat flux vector

The second invariant studied here for demonstrating the SGS effects is the alignment angle between the modelled SGS HF vector h_j and the temperature gradient $\partial\bar{\theta}/\partial x_j$, defined as:

$$\Phi \stackrel{def}{=} \cos^{-1}(h_j, \partial\bar{\theta}/\partial x_j) = \cos^{-1}[(h_j \cdot \partial\bar{\theta}/\partial x_j)/(|h_j| \cdot |\partial\bar{\theta}/\partial x_j|)]. \quad (30)$$

Angle Φ is an important parameter for characterizing a SGS HF model. For the conventional eddy diffusivity type models (e.g., the DEDM-HF, which requires that h_j be aligned with $-\partial\bar{\theta}/\partial x_j$), this alignment angle can only take one of two values: either 0° (when $C_{\theta E} < 0$) or 180° (when $C_{\theta E} > 0$). In the case of $\Phi = 180°$, the physical mechanism for SGS heat flux transfer is analogous to the process of molecular heat conduction governed by Fourier's law. The case of $\Phi = 0°$ is allowed only in a dynamic SGS HF modelling procedure when $C_{\theta E}$ is allowed to be negatively valued. Since the physics of turbulent SGS motions is different than a molecular diffusion/conduction process, the value of Φ is expected to be different than either 0° or 180°. For the DHLTDM-HF, DFLTDM-HF and DNTDM-HF, the value of Φ can vary over a large range due to the introduction of the linear and nonlinear tensor diffusivities inherent in their constitutive relations. Therefore, qualitatively, the value of Φ reflects the degree of

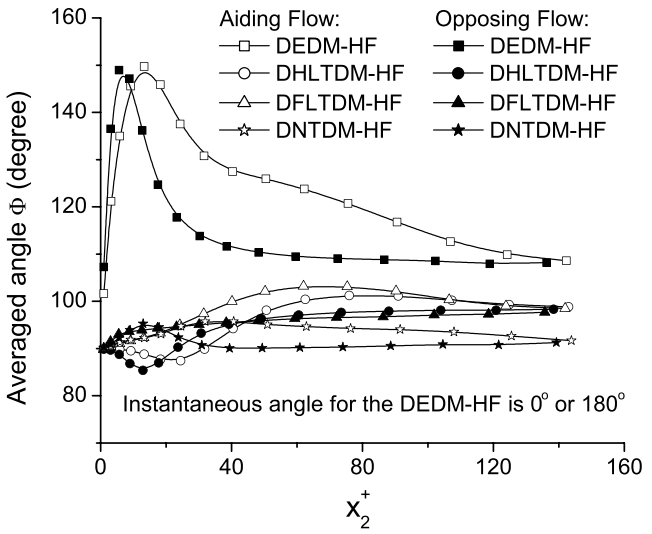

Fig. 13. Averaged alignment angle Φ between h_j and $\frac{\partial\bar{\theta}}{\partial x_j}$.

deviation of the constitutive relation of a SGS HF model from the equivalent of Fourier's law.

Fig. 13 shows the time- and plane-average profile of Φ predicted by four different SGS HF models. In general, the performance of the DHLTDM-HF, DFLTDM-HF and DNTDM-HF are similar. The predicted average value of Φ for these three models varies in the range [85°,101°], [90°,103°] and [90°,96°], respectively, indicating an overall perpendicular alignment pattern between h_j and $\partial\bar{\theta}/\partial x_j$. Furthermore, the averaged value of Φ predicted by these three models converges precisely to 90° at the wall. This is consistent with the physics that in the vicinity of the wall where heat transfer is dominated by the mechanism of molecular heat conduction, the temperature gradient is dominated by its wall-normal component and h_j is approximately parallel to the wall.[1] As shown in Fig. 13, the behaviour of the DEDM-HF is drastically different than that exhibited by the other three SGS HF models. However, it is interesting to observe that due to the self-calibration mechanism inherent in the dynamic modelling procedure, a simple SGS HF model such as the DEDM-HF is also capable of roughly capturing the above analyzed near-wall physics in a time- and plane-averaged sense, since it can be seen from the figure that the averaged value of Φ predicted by the DEDM-HF approaches 102° at $x_2^+ \approx 1$ (which approximates the near orthogonal alignment between h_j and $\partial\bar{\theta}/\partial x_j$ predicted by the other three SGS HF models). However, we must bear in mind that this average value of Φ is generated by blending the two instantaneous modes intrinsic to the DEDM-HF (viz., 0° and 180°), and neither of these two instantaneous modes provides a correct geometrical representation for the actual SGS HF vector.

Figs. 14a and b show the PDF of Φ predicted using the four SGS HF models for the aiding and opposing flow regions in two different layers (with different x_2^+ values). As expected, it is observed in Fig. 14a that the PDF of Φ predicted using the DEDM-HF in the two different flow layers behaves as a bimodal distribution which peaks sharply at $\Phi = 0°$ and 180°. In contrast, for the DHLTDM-HF, DFLTDM-HF and DNTDM-HF, it is observed from Figs. 14b–d that although the most probable states predicted using these three models varies in the central layer, a common mode at $\Phi = 90°$ dominates in the near-wall regions ($x_2^+ = 3.18$ and $x_2^+ = 3.06$ for the aiding and opposing flow regions, respectively). This confirms the previous analysis that in the vicinity of the wall, the temperature gradient vector $\partial\bar{\theta}/\partial x_j$ is dominated by its wall-normal component and h_j is dominated by the components parallel to the wall in an averaged sense. Obviously, such near-wall physics of heat transfer at the subgrid scale can be successfully reproduced by the three SGS HF models based on a tensor diffusivity, but not by the DEDM-HF based on a scalar eddy diffusivity.

5. Conclusions

This paper presents a general approach for the family of dynamic SGS heat flux models based on an explicit algebraic constitutive relation of the form $h_j = f(\overline{S}_{ij}, \partial\bar{\theta}/\partial x_j)$. For this family of dynamic SGS heat flux models, there are only three independent constituent terms proportional to $|\overline{S}|\delta_{jk}\partial\bar{\theta}/\partial x_k$ as the zeroth-order (or the eddy diffusivity) component, $\overline{\Delta}^2\overline{S}_{jk}\partial\bar{\theta}/\partial x_k$ as the first-order component, and $\overline{\Delta}^2\overline{S}_{ji}\overline{S}_{ik}\partial\bar{\theta}/\partial x_k$ as the second-order (or quadratic) component. The proposed DFLTDM-HF is constructed from both the zeroth- and first-order components and corresponds to a general linear tensor diffusivity model for representing the SGS HF; this model includes the conventional DEDM-HF of Moin et al. (1991) and the DHLTDM-HF of Peng and Davidson (2002) as special cases. The second SGS HF model proposed in this research is the DNTDM-HF, which represents the most general approach for SGS HF modelling based on the form $h_j = f(\overline{S}_{ij}, \partial\bar{\theta}/\partial x_j)$; this general model includes the DEDM-HF, DHLTDM-HF and DFLTDM-HF as special cases.

Based on a comparative LES study of a combined forced and natural convective flow, it is confirmed that numerical simulations using the proposed DFLTDM-HF and DNTDM-HF can successfully reproduce prototypical resolved flow and temperature quantities in comparison with the DNS results (Kasagi and Nishimura, 1997; Kuroda et al., 1995). These resolved quantities include the mean and variance of the velocity and temperature fields,

[1] Following the original approach of Leonard (1974) and Clark et al. (1979), and more specifically, following the recent work of Brun and Friedrich (2001), it can be shown using a Taylor series analysis that the SGS HF can be approximated by: $h_j = C\overline{\Delta}^2\frac{\partial\bar{u}_j}{\partial x_k}\frac{\partial\bar{\theta}}{\partial x_k} + o(\overline{\Delta}^2)$. In the vicinity of the wall, $\frac{\partial\bar{u}_j}{\partial x_k}$ is dominated by $\frac{\partial\bar{u}_1}{\partial x_2}$ and $\frac{\partial\bar{u}_3}{\partial x_2}$, and $\frac{\partial\bar{\theta}}{\partial x_k}$ is dominated by $\frac{\partial\bar{\theta}}{\partial x_2}$ in an ensemble-averaged sense. As such, at the wall, the SGS HF and resolved temperature gradient vectors can be approximated as $[h_j]_w \approx C\overline{\Delta}^2[\frac{\partial\bar{u}_1}{\partial x_2}\frac{\partial\bar{\theta}}{\partial x_2}, 0, \frac{\partial\bar{u}_3}{\partial x_2}\frac{\partial\bar{\theta}}{\partial x_2}]^T_w$ and $[\frac{\partial\bar{\theta}}{\partial x_k}]_w \approx [0, \frac{\partial\bar{\theta}}{\partial x_2}, 0]^T_w$, respectively, which indicates that h_j is parallel to the wall and is perpendicular to the resolved temperature gradient, i.e. $[h_j]^T_w \cdot [\frac{\partial\bar{\theta}}{\partial x_k}]_w \approx 0$.

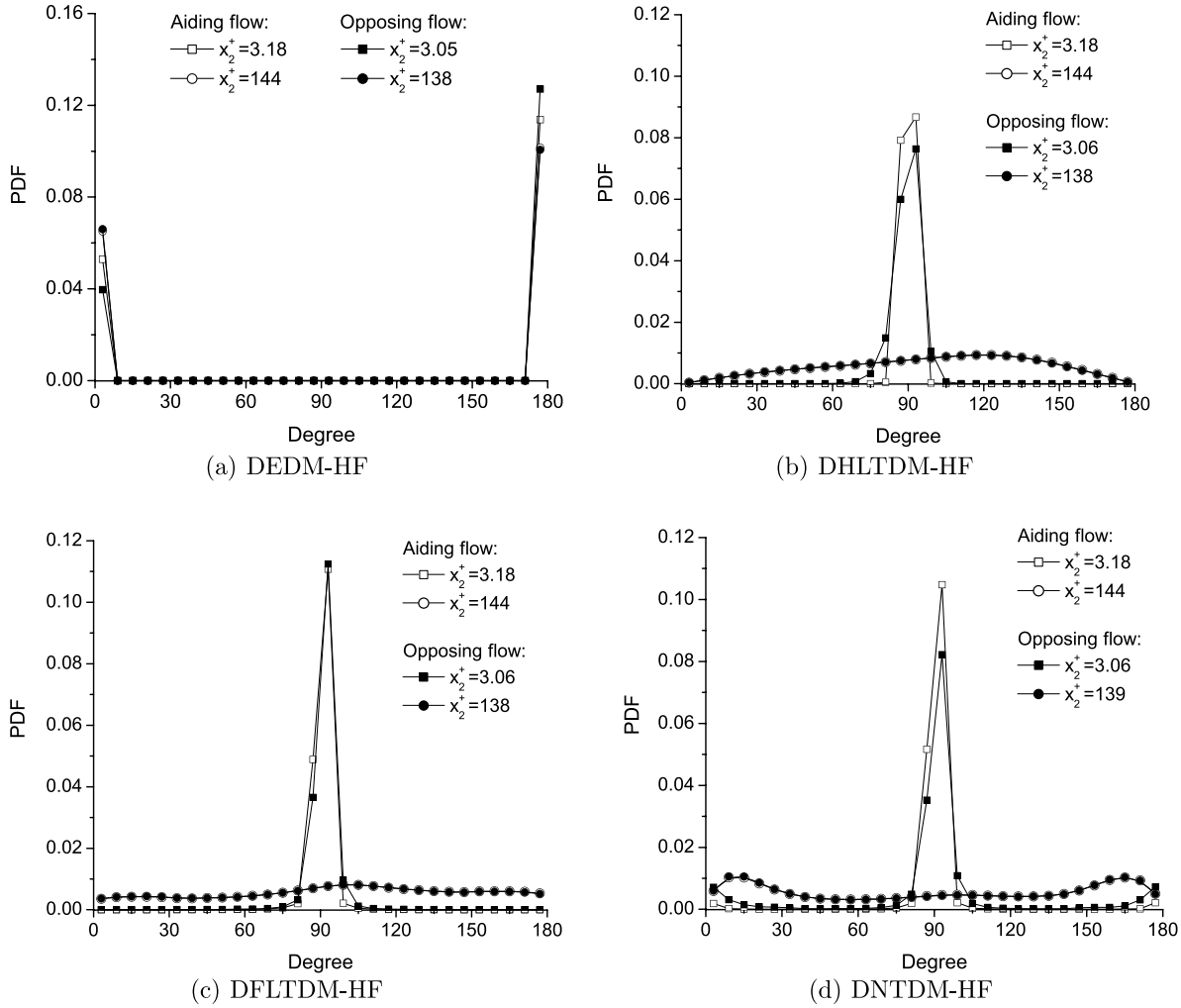

Fig. 14. PDF of the alignment angle Φ between h_j and $\frac{\partial\bar{\theta}}{\partial x_j}$ predicted using different SGS HF models.

and the budget of the shear stresses and heat fluxes. Although slight differences exist, the performance of all four SGS HF models is, in general, similar in terms of their prediction of flow and temperature statistics at the resolved scales. This is because large energetic and flow dependent motions are directly computed at the resolved (or filtered) scales in an LES.

However, at the subgrid-scale, the performance of the four SGS HF models are shown to be different. The conventional DEDM-HF cannot provide a correct instantaneous geometrical representation of the SGS HF vector h_j, owing to its unphysical constitutive constraint which requires the heat flux vector be exactly aligned (either parallel or anti-parallel) with the resolved negative temperature gradient vector. In contrast, the DHLTDM-HF, DFLTDM-HF and DNTDM-HF provide more degrees of freedom in modelling h_j, allow for non-alignment between h_j and $-\partial\bar{\theta}/\partial x_j$, and are able to reproduce the near-wall physics that these two vectors tend to be orthogonally aligned at the wall. It is interesting to observe that although the DEDM-HF fails to reflect this near-wall physics in terms of the PDF of the alignment angle Φ between h_j and $\partial\bar{\theta}/\partial x_j$, it can nevertheless still approximate this near-wall physics in a time- and plane-averaged sense owing to the self-calibration mechanism inherent in a dynamic modelling procedure.

The proposal of the DFLTDM-HF and DNTDM-HF is important in terms of the development of the theory of constitutive relations for SGS HF modelling. Together with DEDM-HF and DFLTDM-HF, they complete the development of dynamic SGS HF models of the general explicit algebraic form $h_j = f(\overline{S}_{ij}, \partial\bar{\theta}/\partial x_j)$. Because the computational time for the numerical simulation is dominated by the pressure solver for the filtered momentum equations, the differences in computational time between different SGS HF modelling approaches are insignificant. Based on the physical and numerical analysis conducted in this research, it is shown that the predictive performances of the DHLTDM-HF, DFLTDM-HF and DNTDM-HF are superior to that of the DEDM-HF, especially at the subgrid scales. However, for the flow simulated in this paper, there appears to be no significant differences in overall predictive performance between the DHLTDM-HF, DFLTDM-HF and DNTDM-HF.

As such, the major difference between different SGS HF modelling approaches investigated here mainly lies in the mathematical and physical aspects of their model formulations and their predictive performances at the subgrid-scale, rather than either their predictive performances at the large resolved scale or the computational costs. On considering the numerical results and complexity of the models, it appears that the DHLTDM-HF and DFLTDM-HF are relatively more attractive among the four SGS HF models tested in this study. In the future, more extensive *a priori* and *a posteriori* LES studies based on different test cases (with different Reynolds and Grashof numbers, and different types of heat and fluid flows) will be required in order to obtain a more comprehensive understanding of the importance of the role of each independent tensorial term appearing in the DFLTDM-HF and DNTDM-HF and also to evaluate the predictive accuracy of these two new SGS HF models.

Acknowledgement

Support from the National Sciences and Engineering Research Council (NSERC) is gratefully acknowledged.

References

Abdelmeguid, A.M., Spalding, D.B., 1979. Turbulent flow and heat transfer in pipes with buoyancy effects. J. Fluid Mech. 94, 383–400.

Avancha, R.V.R., Pletcher, R.H., 2002. Large eddy simulation of the turbulent flow past a backward-facing step with heat transfer and property variations. Int. J. Heat Fluid Flow 23, 601–614.

Brun, C., Friedrich, R., 2001. Modelling of the test SGS tensor T_{ij}: an issue in the dynamic approach. Phys. Fluids 13, 2373–2385.

Cabot, W.H., 1992. Large eddy simulations of time-dependent and buoyancy-driven channel flows. Annual Research Briefs. Center for Turbulence Research, Stanford Univ., pp. 45–60.

Clark, R.A., Ferziger, J.H., Reynolds, W.C., 1979. Evaluation of subgrid-scale models using an accurately simulated turbulent flow. J. Fluid Mech. 91, 1–16.

Dailey, L.D., Meng, N., Pletcher, R.H., 2003. Large eddy simulation of constant heat flux turbulent channel flow with property variations: quasi-developed model and mean flow results. ASME J. Heat Trans. 125, 27–38.

Davidson, L., Čuturić, D., Peng, S.-H., 2003. DNS in a plane vertical channel with and without buoyancy. In: Hanjalić, K., Nagano, Y., Tummers, M.J. (Eds.), Proceedings of Turbulence Heat and Mass Transfer 4 (THMT4). Begell House, Antalya, Turkey, pp. 401–408.

Easby, J.P., 1978. The effect of buoyancy on flow and heat transfer for a gas passing down a vertical pipe at low turbulent Reynolds numbers. Int. J. Heat Mass Trans. 21, 791–801.

Gatski, T.B., Speziale, C.G., 1993. On explicit algebraic stress models for complex turbulent flows. J. Fluid Mech. 254, 59–78.

Germano, M., Piomelli, U., Moin, P., Cabot, W.H., 1991. A dynamic subgrid-scale eddy viscosity model. Phys. Fluids A 3, 1760–1765.

Horiuti, K., 2003. Roles of non-aligned eigenvectors of strain-rate and subgrid-scale stress tensors in turbulence generation. J. Fluid Mech. 491, 65–100.

Jaberi, F.A., Colucci, P.J., 2003. Large eddy simulation of heat and mass transport in turbulent flows, part 2: scalar field. Int. J. Heat Mass Trans. 46, 1827–1840.

Jackson, J.D., Cotton, M.A., Axcell, B.P., 1989. Studies of mixed convection in vertical tubes. Int. J. Heat Fluid Flow 10, 2–15.

Kang, H.S., Meneveau, C., 2002. Universality of large eddy simulation model parameters across a turbulent wake behind a heated cylinder. J. Turbul. 3 (32), 1–27.

Kasagi, N., Nishimura, M., 1997. Direct numerical simulation of combined forced and natural turbulent convection in a vertical plane channel. Int. J. Heat Fluid Flow 18, 88–99, DNS data downloadable from http://www.thtlab.t.u-tokyo.ac.jp/.

Keating, A., Piomelli, U., Bremhorst, K., Nešić, S., 2004. Large-eddy simulation of heat transfer downstream of a backward-facing step. J. Turbul. 5 (20), 1–27.

Kim, J., Moin, P., 1985. Application of a fractional-step method to incompressible Navier–Stokes equations. J. Comp. Phys. 59, 308–323.

Kobayashi, T., 2006. Large eddy simulation for engineering applications. Fluid Dyn. Res. 38, 84–107.

Kuroda, A., Kasagi, N., Hirata, M., 1995. Direct numerical simulation of turbulent plane Couette–Poiseuille flows: effect of mean shear rate on the near-wall turbulence structures. In: Durst, F., Kasagi, N., Launder, B.E., Schmidt, F.W., Suzuki, K., Whitelaw, J.H. (Eds.), Turbul. Shear Flows 9. Springer-Verlag, Berlin, pp. 241–257.

Lee, J.S., Xu, X., Pletcher, R.H., 2004. Large eddy simulation of heated vertical annular pipe flow in fully developed turbulent mixed convection. Int. J. Heat Mass Trans. 47, 437–446.

Leonard, A., 1974. Energy cascade in large-eddy simulations of turbulent fluid flows. Adv. Geophys. 18A, 237–248.

Lilly, D.K., 1992. A proposed modification of the Germano subgrid-scale closure method. Phys. Fluids A 4, 633–635.

Metais, B., Eckert, E.R.G., 1964. Forced, mixed and free convection regimes. ASME J. Heat Trans. 86, 295–296.

Moin, P., Squires, K., Cabot, W., Lee, S., 1991. A dynamic subgrid-scale model for compressible turbulence and scalar transport. Phys. Fluids A 3, 2746–2757.

Nakajima, M., Fukui, K., Ueda, H., Mizushina, T., 1980. Buoyancy effects on turbulent transport in combined free and forced convection between vertical parallel plates. Int. J. Heat Mass Trans. 23, 1325–1336.

Pallares, J., Davidson, L., 2002. Large-eddy simulations of turbulent heat transfer in stationary and rotating square ducts. Phys. Fluids 14, 2804–2816.

Peng, S.-H., Davidson, L., 2002. On a subgrid-scale heat flux model for large eddy simulation of turbulent thermal flow. Int. J. Heat Mass Trans. 45, 1393–1405.

Porté-Agel, F., Pahlow, M., Meneveau, C., Parlange, M.B., 2001a. Atmospheric stability effect on subgrid-scale physics for large-eddy simulation. Adv. Water Resour. 24, 1085–1102.

Porté-Agel, F., Parlange, M.B., Meneveau, C., Eichinger, W.E., 2001b. A priori field study of the subgrid-scale heat fluxes and dissipation in the atmospheric surface layer. J. Atmos. Sci. 58, 2673–2698.

Qin, Z., Pletcher, R.H., 2006. Large eddy simulation of turbulent heat transfer in a rotating square duct. Int. J. Heat Fluid Flow 27, 371–390.

Reiner, M., 1945. A mathematical theory of dilatancy. Amer. J. Math. 67, 350–362.

Rhie, C.M., Chow, W.L., 1983. Numerical study of the turbulent flow past an isolated airfoil with trailing edge separation. AIAA J. 21, 1525–1532.

Rivlin, R.S., 1948. Large elastic deformations of isotropic materials. iv. further developments of the general theory. Philos. Trans. R. Soc. Lond. A 241, 379–397.

Sagaut, P., 2002. Large eddy simulation for incompressible flows: an introduction, second ed. Springer, Berlin.

Salvetti, M.V., Banerjee, S., 1995. A priori tests of a new dynamic subgrid-scale model for finite-difference large-eddy simulations. Phys. Fluids 7, 2831–2847.

Spencer, A.J.M., 1971. Part III: Theory of invariants. In: Eringen, A.C. (Ed.), Continuum Physics, Volume I–Mathematics. Academic, New York.

Speziale, C.G., 1987. On nonlinear k–l and k–ϵ models of turbulence. J. Fluid Mech. 178, 459–475.

Sullivan, P.P., Moeng, C.H., 1992. An evaluation of the dynamic subgrid scale model in buoyancy driven flows. In: Proceedings of the 10th Symp. Turbul. Diffusion, Portland, Oregon, pp. 82–85.

Tanaka, H., Maruyama, S., Hatano, S., 1987. Combined forced and natural convection heat transfer for upward flow in a uniformly heated vertical pipe. Int. J. Heat Mass Trans. 30, 165–174.

Tyagi, M., Acharya, S., 2005. Large eddy simulations of flow and heat transfer in rotating ribbed duct flows. ASME J. Heat Trans. 127, 486–498.

Wang, B.-C., Bergstrom, D.J., 2005. A dynamic nonlinear subgrid-scale stress model. Phys. Fluids 17 (035109), 1–15.

Wang, B.-C., Bergstrom, D.J., Yin, J., Yee, E., 2006a. Turbulence topologies predicted using large eddy simulations. J. Turbul. 7 (34), 1–28.

Wang, B.-C., Yee, E., Bergstrom, D.J., 2006b. Geometrical description of the subgrid-scale stress tensor based on Euler axis/angle. AIAA J. 44, 1106–1110.

Wang, B.-C., Yin, J., Yee, E., Bergstrom, D.J., 2006c. A new irreducible dynamic nonlinear tensor-diffusivity SGS heat-flux model for LES of convective flows. In: Hanjalić, K., Nagano, Y., Jakirlić, S. (Eds.), Proceedings of the 5th International Symposium on Turbulence, Heat and Mass Transfer (THMT5). Begell House, Dubrovnik, Croatia, pp. 315–318.

Wang, B.-C., Yee, E., Yin, J., Bergstrom, D.J., 2007. A general dynamic linear tensor-diffusivity subgrid-scale heat flux model for large-eddy simulation of turbulent thermal flows. Numer. Heat Trans.: Part B 51, 205–227.

Wang, L., Lu, X.Y., 2004. An investigation of turbulent oscillatory heat transfer in channel flows by large eddy simulation. Int. J. Heat Mass Trans. 47, 2161–2172.

Winckelmans, G.S., Jeanmart, H., Carati, D., 2002. On the comparison of turbulence intensities from large-eddy simulation with those from experiment or direct numerical simulation. Phys. Fluids 14, 1809–1811.

Wong, V.C., Lilly, D.K., 1994. A comparison of two dynamic subgrid closure methods for turbulent thermal convection. Phys. Fluids 6, 1016–1023.

Yan, Z.H., 2003. A numerical study of effect of initial condition on large eddy simulation of thermal plume. Numer. Heat Trans.: Part B 43, 167–178.

Zang, Y., Street, R.L., Koseff, J.R., 1993. A dynamic mixed subgrid-scale model and its application to turbulent recirculating flows. Phys. Fluids A 5, 3186–3196.

Zhang, W., Chen, Q., 2000. Large eddy simulation of natural and mixed convection airflow indoors with two simple filtered dynamic subgrid scale models. Numer. Heat Trans.: Part A 37, 447–463.

Zheng, Q.S., 1994. Theory of representations for tensor functions—a unified invariant approach to constitutive equations. Appl. Mech. Rev. 47, 545–587.